Cellulose based pH-sensitive hydrogel for highly efficient dye removal in water treatment: kinetic, thermodynamic, theoretical and computational studies

Jabir Loubna, El-Hammi Hayat, Mohammed Nor, Jilal Issam, El Idrissi Abderrahmane, Amhamdi Hassan, Abou-Salama Mohamed, El Ouardi Youssef, El Barkany Soufian, Laatikainen Katri

DOI: 10.1007/s10570-022-04564-z

Cellulose based pH-sensitive hydrogel for highly efficient dye removal in water treatment: kinetic, thermodynamic, theoretical and computational studies

Loubna Jabir*[a], Hayat El-Hammi[a], Nor Mohammed[b], Issam Jilal[a], Abderrahmane El Idrissi[c], Hassan Amhamdi[b], Mohamed Abou-Salama[a], Youssef El Ouardi[d,e], Soufian El Barkany*[a], Katri Laatikainen[e]

[a] *Laboratory of Molecular Chemistry, Materials and Environment (LMCME), Department of Chemistry, Faculty Multidisciplinary Nador, Mohamed 1st University, P. B. 300, Nador 62700, Morocco.*
[b] *Applied Chemistry Unit, Sciences and Technologies Faculty, Abdelmalek Essaadi University, 32 003 Al Hoceima, Morocco*
[c] *Laboratory Applied Chemistry and Environmental (LCAE-URAC18), Faculty of Sciences of Oujda, Mohamed1stUniversity, 60000 Oujda, Morocco*
[d] *LIMOME Laboratory, Sidi Mohamed Ben Abdellah University, Faculty of Sciences Dhar El Mehraz, Dhar El Mehraz B.P. 1796 Atlas, Fes 30000, Morocco*
[e] *Lappeenranta University of Technology, Laboratory of Separation Technology, P.O. Box 20, FI- 53851 Lappeenranta, Finland.*

**Corresponding authors. E-mail addresses: el.barkany011@gmail.com (Soufian El Barkany), ja.loubna@gmail.com (Loubna Jabir)*

Abstract:

In this paper, a new green pH-sensitive EDTA crosslinked HEC (cellulose-based hydrogel (swelling rate ~ 1005 %)) adsorbent was successfully elaborated. The synthesis of HEC-EDTA at the high advanced crosslinking degree (up to 92 %), was carried out using DAEDT and DMAP as acyl transfer agent, where the lamellar morphology (2D-microstructure) was highly suggested based on the average functionality of the reaction system. The crosslinking degree was confirmed using structural analyzes (FTIR and 13C CP/MAS-NMR) and elemental profile analysis. The new EDTA crosslinked HEC demonstrated a high uptake capacity (~2000 $mg.g^{-1}$) to aquatic micropollutants, especially methylene blue as cationic dyes model. The kinetic study showed that the adsorption process was well described by the pseudo-second-order kinetic, while the thermodynamic parameters exhibited a negative effect of temperature indicating a physical adsorption process. In addition, the adsorption capacity was studied varying to the experimental conditions (pH, contact time, concentration, etc.), and the Freundlich model revealed a strong correlation to the experimental data indicating an energetic heterogeneity of the surface active sites. Furthermore, using COMPASS II, the molecular dynamics (MD) simulations were conducted to optimize the chemical system, where the results showed the predominance of non-covalent molecular adsorbent-adsorbate interactions, which governs cluster design and configurations.

Keywords: *Cellulose adsorbent, pH-sensitive hydrogel, Dyes removal, Water treatment, and Molecular Dynamics*

Introduction

Organic pollutants are molecules defined by their properties of toxicity and persistence in the environment, as well as their bioaccumulation, they have harmful impact on human health and the environment, and are very difficult to get removed by natural biological degradation *(Pagga and Brown 1986, Pelalak, Soltani et al. 2021)*. Depending on their reactivity, hazardous molecules (e.g. pesticides, dyes, hydrocarbons, phenol and its derivatives.) accumulate in living tissues and their concentrations increase along the trophic chain. While most dyes are not directly toxic but many of their metabolites is very harmful *(Naidja 2010)*. Indeed, their mutagenic, teratogenic or carcinogenic effects appear after degradation of the initial molecule into oxidation by-products, such as carcinogenic amine from azo *(Tsuda, Matsusaka et al. 2000)* and leuco derivative from triphenylmethanes *(Culp, Beland et al. 2002)*. These carcinogenic groups (in electrophilic or radical form) attack the DNA and RNA pyrimidic bases altering the genetic code causing mutation and risk of cancer. For example, azo dyes are characterized by the presence of an azo group (–N=N–), where the breaking of the azo bonds leads to the formation of primary amines. These cause *methemoglobinemia*, which is characterized by an impairment of oxygen transport in the blood *(Greene and Baughman 1996)*. Currently, organic dyes that result from anthropogenic activities released into the natural environment is estimated at 15 to 20% of world production *(Salah 2012)*. Organic dyes are pollutants that pose a significant risk to the environment. In particular, industrial effluents from textile activities, such activities often present a large pollutant load that is difficult to biodegrade and that has harmful impacts on the environment and humans *(Danel 1999, Rafatullah, Sulaiman et al. 2010, Gobi, Mashitah et al. 2011)*. The discoloration of textile effluents is often carried out on natural adsorbents, in particular activated carbon *(Malik 2003)*, clay *(Weng and Pan 2007)* and phosphates *(Barka, Qourzal et al. 2008)* but their effectiveness often remains unsatisfactory.

Methylene blue (MB), derived from phenothiazine that occurs in several hydrated forms, is an intensively used cationic dye. The stable molecular structure of MB is the major advantage of its common use as an organic contaminant model *(Wilson 1907, Marr, Stewart et al. 1973, Dutta, Mukhopadhyay et al. 2001, Uddin, Islam et al. 2009, Huang, Chen et al. 2010, Rafatullah, Sulaiman et al. 2010, Sukumaran and Ramalingam 2011, Sbai, Oukili et al. 2016),(Cenens and Schoonheydt 1988, Bolotin, Baranovsky et al. 2006), (Beer, Baumann et al. 2006, Huang, Chen et al. 2010, Rager, Geoffroy et al. 2012)*.

During the last decades, remarkable efforts have been made to eliminate or reduce the polluting load of industrial effluents including coagulation-fluctuation (Vandevivere, Bianchi et al. 1998, Barclay and Buckley 2000), precipitation (Pan, Wang et al. 2016), reverse osmosis *(Li, Lin*

et al. 2011), advanced oxidation processes (POA) *(Andreozzi, Caprio et al. 1999, Crini, Badot et al. 2007, Chergui 2010)*, aerobic *(Hitz, Huber et al. 1978, Hu 1996, Cha, Doerge et al. 2001)* and anaerobic treatments *(Al-Kdasi, Idris et al. 2004)*. These methods have shown limiting drawbacks and obstacles to their application such as high cost; efficiency dependence to types of dyes (i.e. azo), clogging of filters, generation of highly oxidizing radical species, and the formation of more toxic intermediate compounds. The adsorption of organic dyes on solid supports remains very limited at the surface of the adsorbent that requires optimum morphology and large specific surface area. The use of pH- sensitive hydrogels increases the contact surface and allows the penetration of the contaminated solution and through a simple modification of pH facilitates the regeneration of both the organic pollutant and the hydrogel. This is a non-destructive technique that does not require expensive subsequent regeneration and post-treatment of solid waste *(Mckay, Ramprasad et al. 1987)*.

Faced to environmental constraints that require the ecofriendly aspect of industrial processes, several studies have focused on the development of materials of natural origin, such as chitin *(Cao, Pan et al. 2018)*, chitosan *(Melo, Paulino et al. 2018, Kellner-Rogers, Taylor et al. 2019)*, and cellulose *(Senna, Novak et al. 2013, Senna, Novack et al. 2014, Melo, Paulino et al. 2018)*. However, the thermal degradation of cellulose before its melting temperature limits its treatment by thermal processes, whereas its insolubility in almost all usual solvents constitutes a major obstacle to chemical modifications of cellulose by simple reaction routes. The introduction of new functionalities into the polysaccharide structure of cellulose requires complex, expensive and toxic solvation systems *(Jilal, El-Barkany et al. 2019)*. Therefore, the use of cellulose derivative such as cellulose acetate *(TABAGHT, EL IDRISSI et al. , Tenorio-Alfonso, Sánchez et al. 2019)*, ethyl cellulose *(Ma, Gong et al. 2018)* and carboxymethyl cellulose *(Naderi, Lindström et al. 2015, Li, Mei et al. 2016, Hasan, Waibhaw et al. 2018, Rao, Ge et al. 2018)* as intermediate polymers holds promise for the development of new families of cellulose adsorbents. Recently, hydroxyethylcellulose (HEC) a nonionic and water-soluble cellulose derivative has received attention for its excellent performance properties as thickener *(Coryell 2017, Luo, Liu et al. 2018)*, binder *(De Guzman and Balela 2019, Hämmer, Gassmann et al. 2019, Younes, El-sharkawy et al. 2019)*, emulsifier *(Wang, He et al. 2020, Yang, Li et al. 2020)*, cement set retarder *(Zhi, Ma et al. 2017, Liu, Wang et al. 2019)* and flocculent to colloidal turbidity and heavy metals removal *(Jilal, El Barkany et al. 2018, Chaouf, El Barkany et al. 2019, Jilal, El-Barkany et al. 2019)*.

In addition, the chemical structure of HEC is comparable to that of cellulose, where the introduction of ethyl groups causes the supramolecular intercalation of macromolecular chains

which decreases the density of hydrogen bonds, and increases its reactivity increasing the density of primary hydroxyls. These structural properties solve the problem of solubility and therefore the feasibility of chemical modification, resulting in a wide variety of cellulosic materials based on HEC including heavy metal adsorbents *(Choudhury, Majumdar et al. 2018, Jin, Easton et al. 2018)* and materials for dyes removal *(Huang, Wu et al. 2019, Ning, Zhang et al. 2020).*

The material discussed in this article has never been discussed in previous literature, neither in terms of synthesis and characterization nor of the application as an adsorbent that proven the originality and the credibility of this work. Therefore, the aim of this study was to design new green pH-sensitive cellulose-based hydrogel adsorbent. A very effective method for easily cross-linking HEC using ETDA as a cross-linker is adopted for reaching this objective. FTIR and ^{13}C-CP/MAS NMR analysis were in good correlation with the proposed chemical structure of such hydrogel. The effects of pH, contact time, concentration on dye adsorption were investigated and discussed by summarizing the kinetic and isotherm adsorption studies to evaluate the adsorption capacity of HEC-EDTA material. The composition has shown a high adsorption capacity of dyes in the optimal experimental conditions.

Materials and methods:

Materials:

Hydroxyethyl Cellulose (HEC, DS = 1.5) and methylene blue (MB) were obtained from Sigma Aldrich. Ethylenediaminetetraacetic acid (EDTA), 4-dimethylaminopyridine (DMAP) and dimethyl sulfoxide (DMSO) were purchased from Honeywell *Riedel-de-Haën™*. The other solvents and chemicals are of analytical grades and were received from Sigma Aldrich where they were used without further purification.

Methods:

FTIR spectra are recorded between 400 cm^{-1} and 4000 cm^{-1} on *FTIR-RShimadzu* type spectrometer using the pellets method, where 1% w of the sample was finely ground with 99% w of spectroscopy grade KBr, 40 scans were performed for each analysis at 2 cm^{-1} resolution. The absorbance was calculated from Uv-vis spectra performed on a *Uv-Shimadzu* type spectrophotometer using quartz cuvettes at the wavelength of 665 nm. UV-vis spectra were recorded in the wavelength range of 400 nm to 800 nm. The elemental analyses results were achieved using *Perkin Elmer Series II CHNS/O Model 2400* analyzer.^{13}C NMR spectra acquired

with Cross-Polarization Magic Angle Spinning (solid-state CP/MAS 13C NMR) spectrum was recorded on a *Bruker DRX-400* spectrometer with a frequency of 100 MHz, and 1800 scans were recorded with the 90° pulse time of 4.85 μs at room temperature. The acquisition and the delay time were 0.032 s and 2 s, respectively. The surface charge of materiel was evaluated using the zeta potential (ζ) against pH (2 – 11) in Milli-Q water at 0.1%, and the results were recorded at 25 ± 0.1 °C using *Zetasizer Nano ZS (Malvern Instruments)*.

Preparation of HEC-EDTA:

3 g (13.16 mmol) of HEC in 40 ml of DMSO were slowly added by an addition funnel to 5 g (19.51 mmol) of EDTAD (prepared according to the method described by *Capretta et al.(Capretta, Maharajh et al. 1995, Júnior, Gurgel et al. 2009, Senna, Novack et al. 2014)* and 0.5 g (4 mmol) of DMAP as catalyst (acyl transfer reagent) dissolved in 15 ml of DMSO, and the reaction mixture was stirred for 4 h at 60 ˚C. At the end of the reaction, HEC-EDTA was precipitated in acetone, filtered under vacuum, washed with acetone, thus a white powder was obtained which became gelatinous after washing with a saturated sodium bicarbonate solution of $NaHCO_3$.

Measurement of swelling degree:

The swelling degree (S %) was determined according to ASTM, 1979 and ASTM1239-55. In short, the gels (0.1 g) were immersed in deionized water and taken out at different consecutive time intervals. After equilibrium, the swollen samples were separated using a 100-mesh filter-bag and dried to drain the excess water. Then, the swollen samples were weighed and the swelling degree (S %) of the hydrogel was calculated according to the following equation (Eq. 1) :

$$S(\%) = (W_e - W_i)/W_i \ (Eq. 1)$$

Wi and *We* are the initial weight of the dried hydrogel (g) and the weight of gel at equilibrium (g).

Adsorption experiment:

MB adsorption experiments on HEC-EDTA were performed in the range of initial concentrations of 10 $mg.L^{-1}$ to 600 $mg.L^{-1}$ of aqueous MB solutions. The kinetic study was

performed by varying the contact time from 0 to 40 minutes. The batches were carried out by stirring a quantity of 30 mg of HEC-EDTA gel in 10 ml of MB solution, and the pH was set at a value of 8 for 30 min as a contact time. The effect of pH (2 – 11) and gel dose (0.15 – 0.6 g. L^{-1}) on adsorption capacity were investigated. However, the thermodynamic study was carried out in a temperature range of 20 to 60 °C. The concentration of MB before and after adsorption was determined by measuring the absorbance of the solution at λ_{max} = 662 nm, while the adsorption capacity per unit mass of HEC-EDTA and the removal rate (R %) were calculated from equations 2 and 3, respectively.

$$q = (C_0 - C_e).V/M \qquad (Eq.2)$$

$$R(\%) = 1 - C_e/C_0 \qquad (Eq.3)$$

Where, q (mg. g^{-1}) is the equilibrium adsorption capacity at thermodynamic equilibrium, C_0 (mg. L^{-1}) and C_e (mg. L^{-1}) are the initial and the equilibrium concentration of the MB solution, respectively. V (l) is the volume of the MB solution and M (g) is the weight of the HEC-EDTA adsorbent.

Results and discussions:

Synthesis and characterization of HEC-EDTA:

The crosslinking of HEC by EDTA was carried out to modify its hydrophilic character and to prevent its solubility in water. This modification allows HEC-EDTA to be used as an adsorbent for the present micropollutants in aquatic environments (liquid-solid extraction). In this study, the crosslinking was carried out by creating ester bridges between the primary hydroxyl groups of HEC and EDTA. However, to increase the reactivity of the carboxylic functions of EDTA, a trans-anhydridation reaction between EDTA and acetic anhydride was carried out. The functionalization of HEC was carried out in DMSO as a homogeneous medium in the presence of DMAP as an esterification agent. A notable increase in the viscosity of the reaction medium was illustrious during the reaction, which indicates the supramolecular crosslinking of the cellulosic chains (Fig. 1a). EDTA crosslinked HEC hydrogel was recovered in its acidic form by precipitation in acetone and frequent washing with the same solvent and deionized water. In addition, to release the carboxylate functions, the treatments of HEC-EDTA powder with a saturated sodium bicarbonate solution (and then by deionized water until the filtrate neutralization) have caused a radical change in the appearance of the product that became, more and more, gelatinous.

Fig. lb shows the kinetic study of swelling of the HEC-EDTA hydrogel at 25 °C. The significant swelling rate observed from the first contact with the solvent (H_2O) at 40 min can be attributed to the highly hygroscopic character of the sodium EDTA and its instability when exposed to moisture *(Gbadamosi, Famuwagun et al. 2018)*. In addition, the hydrophilic behavior of HEC and its good solubility in the aquatic environment significantly improved the water absorption of the hydrogel. Then, the crosslinking by EDTA prevented the water solubility of HEC, which could enhance the steric stability to retain more water in the network *(Calcagnile, Sibillano et al. 2019)*, and consequently, the rate of swelling increased gradually with time of immersion to reach a maximum value of 950 to 1005 % after 35 min. In the case of functional hydrogels envisioned for ecological applications including processes for removing the pollutant load from industrial effluents, the high swelling and the hygroscopic nature increase the internal surface area favoring better penetration allowing more adsorption sites to be fully exposed to pollutants *(Elbedwehy and*

Atta 2020).

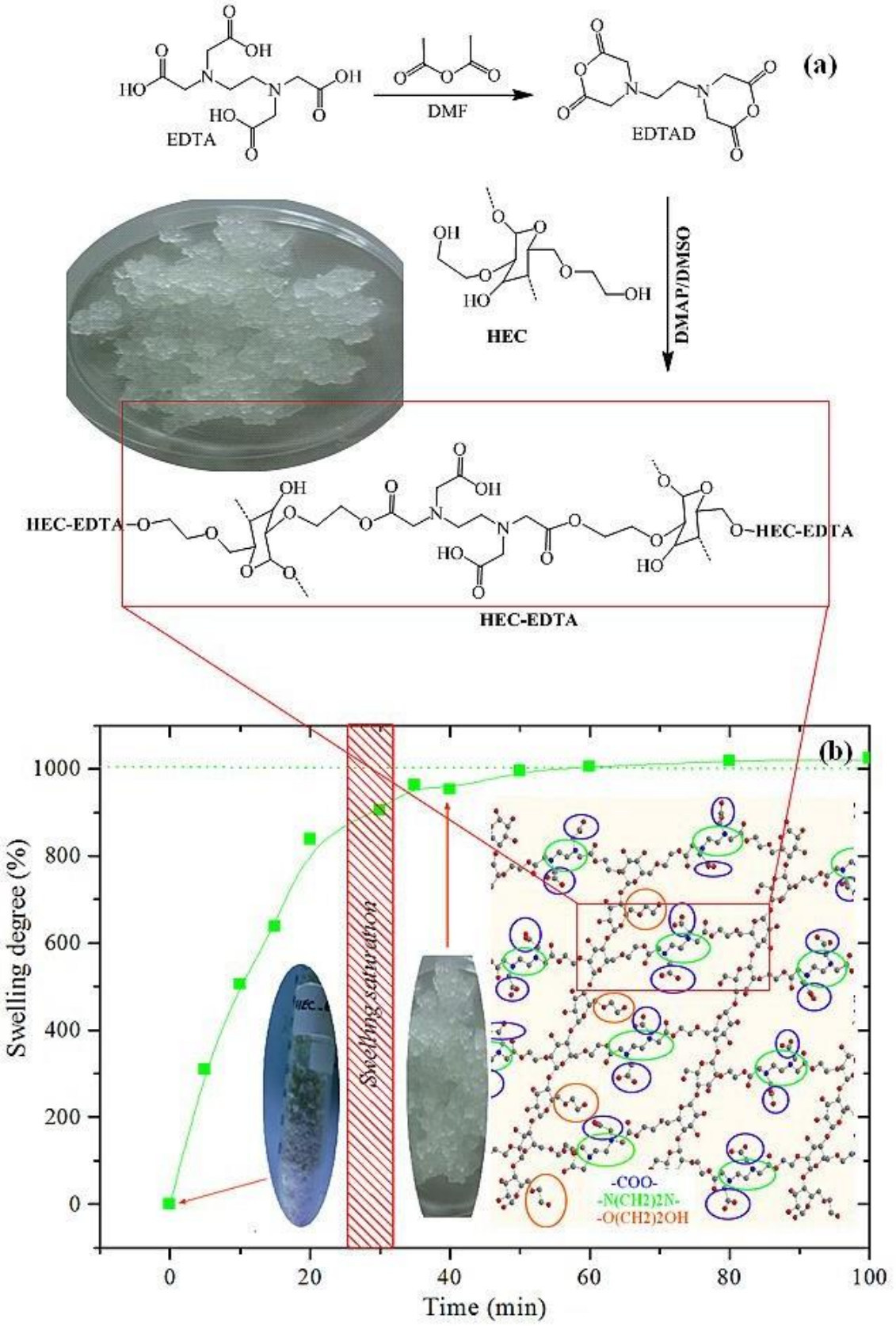

Fig. 1. a) HEC-EDTA synthesis reaction scheme and b) Degree of swelling against emersion time of EDTA crosslinked HEC hydrogel

Fig. 2a represents the FTIR spectra of untreated (EDTA) and treated EDTA (EDTAD). The treatment of EDTA with acetic anhydride showed remarkable changes in the general vibrational aspect of EDTA. On the EDTAD FTIR-spectrum, the appearance of new absorption bands, between 1761 cm^{-1} and 1809 cm^{-1} assigned to the anhydride carbonyl (CO) vibrations (symmetric and antisymmetric), indicate that the trans-anhydridation reaction between EDTA and acetic anhydride was carried out successively. Fig. 2b shows the vibrational spectra (FTIR) of unmodified HEC and HEC-EDTA before and after saponification using a saturated sodium bicarbonate solution.

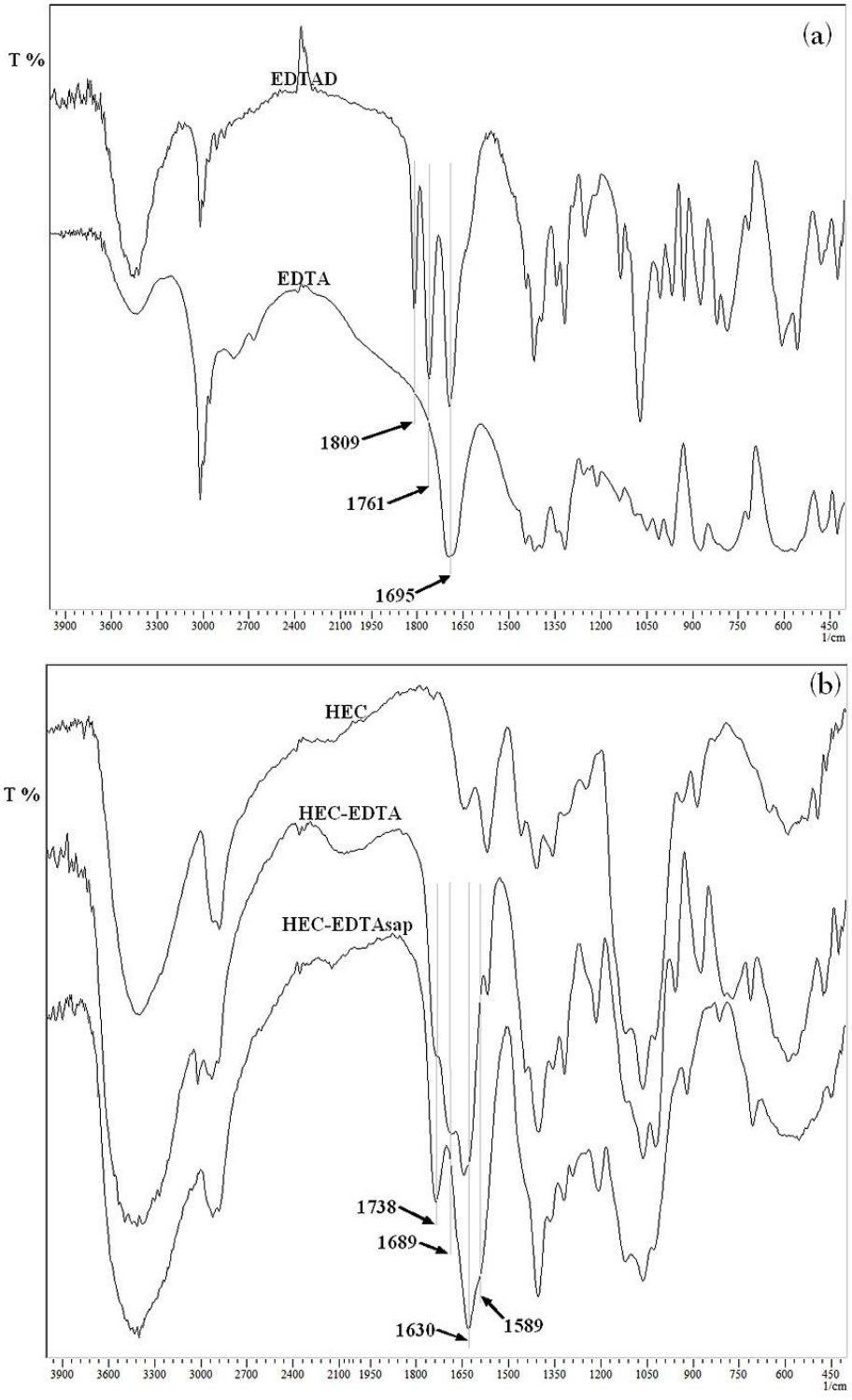

Fig. 2. FTIR spectra of (a) acid and anhydride forms of EDTA and (b) HEC-EDTA and saponified HEC-EDTA

The spectrum of HEC indicates strong adsorption band intensity at 3412 cm^{-1} characteristic of the OH hydroxide group of polysaccharides structures *(Pradeep 2009)*, while the distinguished band around 1355 cm^{-1} is attributed to the deformation vibrations in the plane ofthe OH function of the alcohol group *(Zafar, Aqil et al. 2007)*. The absorption band located at 1060 cm^{-1} corresponds

to COC stretching vibration in glucopyranose *(Silverstein, Bassler et al. 1991)*, where that around 1120 cm^{-1} has been attributed to the asymmetric CO vibration *(Zare, Motahari et al. 2018)*. The spectrum corresponds to HEC-EDTA highlights the esterification reaction via the appearance of new absorption bands characteristic of grafted entities (EDTA). However, the band observed at 1689 cm^{-1} is attributed to the acid carboxylic carbonyl groups (CO), while the band located at 1630 cm^{-1} corresponds to the deformation of naturally absorbed water. The appearance of a new absorption band located at 1738 cm^{-1} corresponds to the carbonyl ester group reveals the successful grafting of EDTA on HEC. After saponification, the shift of the band attributed to the acid carbonyl from 1689 cm^{-1} to 1589 cm^{-1}. This shift indicates the transformation to the carboxylate form (COO^-, Na^+) of carboxylic acid under the action of $NaHCO_3$. This is another strong indication of the incorporation of the carboxylic functions on the surface of the cellulosic material (HEC). The creation of the negatively charged character (carboxylate) is an encouragement to consider HEC-EDTA as a promising candidate to be effective adsorbent for the removal of cationic dyes like MB.

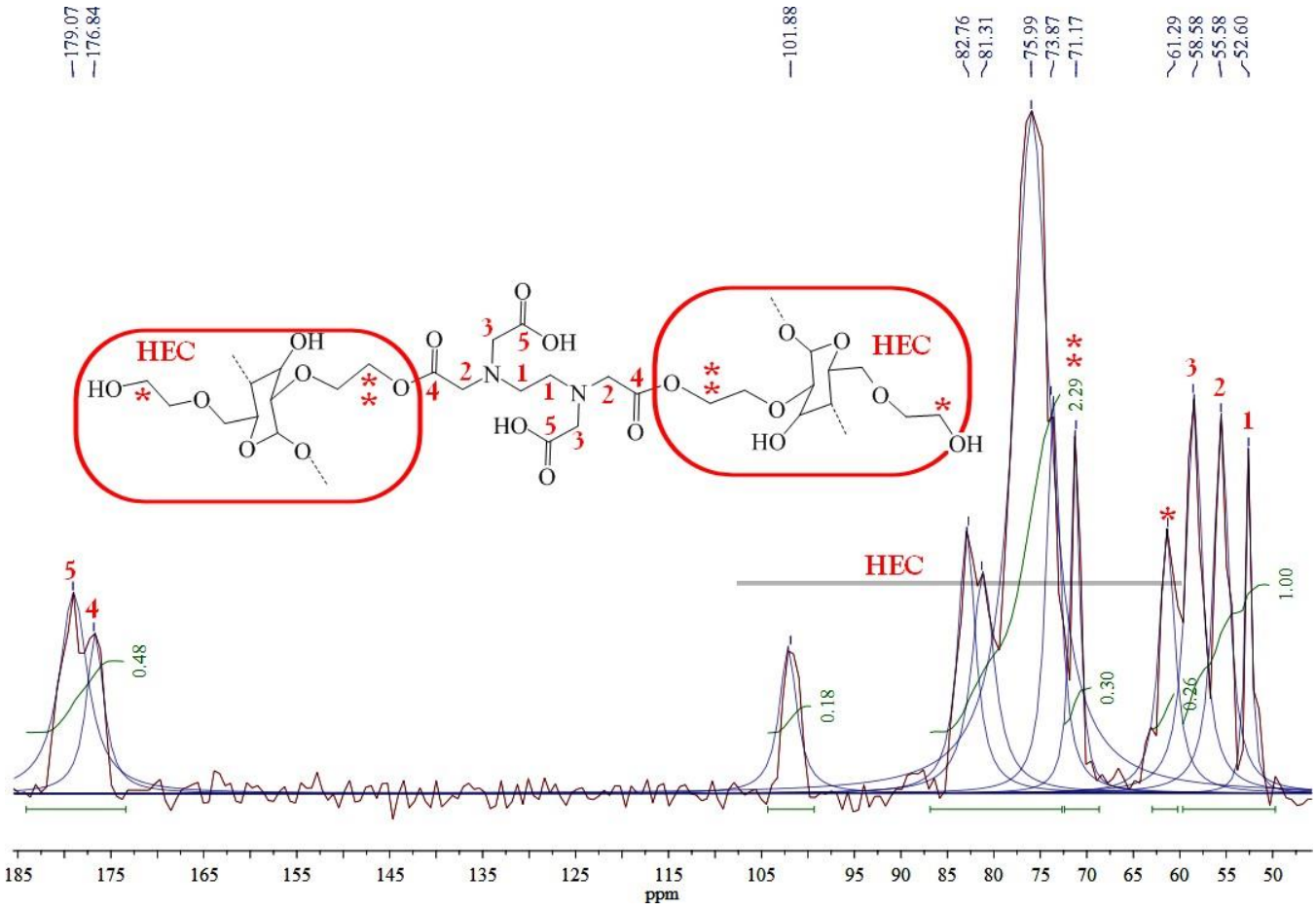

Fig. 3. Solid-state CP/MAS 13C-NMR spectrum of HEC-EDTA

The solid-state CP/MAS ^{13}CNMR spectrum of HEC-EDTA (Fig. 3) reflects the various structural modifications of HEC resulting from EDTA crosslinking reaction. The number of Hydroxyethyl groups (DS) in the starting material (HEC) is estimated in our previous papers basing on the integrations of proton signals of ^{1}H NMR spectra *(Jilal, El Barkany et al. 2018, Chaouf, El Barkany et al. 2019)*. This result was exploited to calculate the degree of substitution of EDTA in this work (DS_{EDTA}). Broad-ringed cellulose skeletal carbon (HEC) signals are recorded between 60 and 105 ppm *(Jilal, El Barkany et al. 2018)*. However, the appearance of new methylene carbon signal at 71.2 ppm (**) is attributed to the chemical shift of typical methylene carbon signals of HEC-linked-EDTA at 61.3 ppm (*), which is a strong signal of the change in the (*) carbon chemical environment, caused by EDTA chemical modification of HEC, proving the successful grafting reaction. Furthermore, the value of DS_{EDTA} ($\simeq$ *0.8)* was calculated from the ^{13}C NMR spectrum of the HEC-EDTA sample shown on Fig. 3, using the following equation (*Eq. 4*) that was established basing on the integrations of the carbonic signals I * *($\simeq$ 0.26)* and I ** ($\simeq$ 0.30):

$$DS_{EDTA} = 1.5\ \frac{I^{**}}{I^{**} + I^{*}} \qquad (eq.4)$$

The ^{13}C solid NMR spectrum (Fig. 3) reveals evidence of grafting and crosslinking reaction by examining the ratio of signal integrations of carbonyl esters binding EDTAentities grafted to HEC chains, which are located at 176.8 ppm (4), and those of free carbonyl acids detected at 179.1 ppm (5). Values close to I_4 (0.23) and I_5 (0.25) indicate a high crosslinking density. Besides, the degree of crosslinking *(Dc %)* is estimated to be around 92 % using the equation 5 (Eq. 5) :

$$D_C(\%) = \left(3 - 4\ \frac{I_5}{I_5 + I_4}\right) \times 100 \qquad (Eq.\ 5)$$

This trend, corresponding to the high level of crosslinking, is confirmed by the closest values of the integrations of the signals attributed to the methylene carbons of the grafted EDTA at 52.6, 55.6 and 58.6 ppm (Fig. 3) assigned to the EDTA carbons (1), (2) and (3), respectively. Furthermore, the integration ratio close to the value 1 between the two typical peaks (2) in α-ester and (3) in α-acid is strong indication of the predominance of the crosslinking aspect of hydrogel.

Besides the NMR, spectral results of HEC-EDTA reported in Fig. 3 confirm those obtained by FTIR vibrational spectroscopy (Fig.2a). In addition, the proposed structure of the new hydrogel developed in this paper is confirmed and is completed by the study of the elemental profile for a DS_{EDTA} of 0.8, and the results are reported in Table 1. Before studying of the elemental profile, there is a need to note that the elemental composition is susceptible toward the structure and bonding variability of the hydrogel network. The experimental data, from the elemental analysis of hydrogel (HEC-EDTA^{a}), showed that the EDTA crosslinking reaction slightly decreased the rate of carbon from 47.37 to 47.23% and that of hydrogen from 7.02 to 6.36 %. Whereas the appearance of higher nitrogen content (3.05 %) compared to the HEC starting material (0 %) could prove the introduction of EDTA as a crosslinking agent.

Table 1. Elemental analysis of HEC and HEC-EDTA$_{0.8}$

	Atomic wt. %

	C	N	H	DS_{EDTA}	$D_{C\,\%}$
HEC	47.37	0.00	7.02	0.00	0.00
HEC-EDTA[a]	47.23	3.05	6.36	0.80	92.0
HEC-EDTA[b]	47.22	3.39	6.30	0.80	100
HEC-EDTA[c]	45.60	5.01	6.08	0.80	0.00

[a]: Synthesized in this work, [b]: Completely crosslinking and [c]: Without crosslinking

On the other hand, the theoretical elemental compositions (HCN) of HEC-EDTA hydrogel at the extreme values of the crosslinking (HEC-EDTA^b for Dc = 100 % and HEC-EDTA^c for Dc = 0 %) have been calculated. Thus, it was noted that the elemental analysis profile for the same degree of substitution (DS_{EDTA} = 0.80), and for a crosslinked polyfunctional samples (as in the case of polysaccharides), is strongly affected by the degree of crosslinking (Dc %). This result can be explained considering the superficial and the core network EDTA distribution in hydrogel materials. Since, in the highest degree of crosslinking, the sharing of each EDTA unit between two AGUs is more considered, while in the materials with lower Dc%, each AGU keeps its EDTA unit. In the case of HEC-EDTA, it is acceptable to have greater value of nitrogen content (5.01 %) for a free system (without crosslinking) and around half (3.39 %) in the case of a fully crosslinked system, indicating that the EDTA moiety is inversely proportional to the degree of crosslinking. In fact, the elemental analysis experimental data were very close to those theoretical characterizing a fully crosslinked system at a DS_{EDTA} value equal to 0.80. This confirms the high Dc % value of 92 % characteristic of the gelatinous system in this work. In comparison with the recently published results *(Zannagui, Amhamdi et al. 2020)*, drastic differences can be caused, by the variation of the values of DS and Dc %, in terms of physicochemical properties particularly the powder-gel aspect, water solubility, swelling, accessibility, etc.

Application of HEC-EDTA to dyes removal in Water Treatment

Effect of contact time and kinetic study

The adsorption kinetic describes the variation of the concentration of adsorbate in the solution as a function of contact time. In order to determine the mechanism limiting the kinetics of the adsorption process, three models were applied during this study, the pseudo- first order, the pseudo-second order and the interparticle diffusion models. Fig. 4a shows the contact time effect on the evolution of MB adsorption capacity of HEC-EDTA, where the initial concentration of cationic dye (C_0) was set at 300 mg. L^{-1}, pH8 and 30 mg of gel- adsorbent. The adsorption kinetic behavior of MB on HEC-EDTA is characterized by a high rate in the initial stage (first 10 min) indicating high accessibility to the adsorption sites, and then the adsorption process progressed with a low increase of the adsorption capacity to reach the equilibrium. The time to equilibrium was 30 min as the optimal contact time, and the maximum adsorption capacity was around 953 mg. g^{-1}.

At the kinetic level, in the pseudo first order model, the adsorption rate is proportional to the variation of the adsorption capacity between the equilibrium and at the t time (*Eq. 6*), k_1 is the rate constant (min^{-1}). By integrating and applying the initial conditions ($t_0=0 \rightarrow q_t=q_0=0$ and $t=t_e \rightarrow q_t=q_e$) the previous equation takes the following linear form (Eq. 7), k_1 and q_e are obtained by plotting ln ($q_e - q_t$) against time. On the other hand, the pseudo second order model gives the adsorption rate proportionally to the square variation of the adsorption capacity between the equilibrium and at the t time (*Eq. 8*), k_2 is the rate constant ($g.mg^{-1}.min^{-1}$). However, the linear form *(Eq. 9)* of the previous equation *(eq. 8)* was obtained by integrating and applying the initial conditions ($t_0=0 \rightarrow q_t=q_0=0$ and $t=t_e \rightarrow q_t=q_e$), q_e and k_2 are obtained by plotting $t/q_t = f(t)$.

$$\frac{dq_t}{dt} = k_{1(}q_{e-}q_{t)} \qquad (eq.\ 6)$$

$$\ln(q_{e-}q_t) = lnq_e - k_1 t \qquad (eq.\ 7)$$

$$\frac{dq_t}{dt} = k_2(q_e - q_t)^2 \qquad (eq.\ 8)$$

$$\frac{t}{qt} = \frac{1}{k_2 {q_e}^2} + \frac{1}{q_e}.t \qquad (eq.\ 9)$$

$$q_t = k_{int}.t^{1/2} + C \qquad (eq.\ 10)$$

To investigate the kinetic profile of MB adsorption onto HEC-EDTA gel, the kinetic data were fitted according to the linear form of pseudo-first-order and pseudo-second-order kinetic models

hence the conventional linear regression of the kinetic results for the two kinetic models are shown in Figure 4a. The comparison of the coefficient of correlation (R) of the linear regression was carried out to confirm the validity of the kinetic models and to examine the absorption kinetic process. Thus, kinetic parameters results of the two models, summarized in table 2, show that the pseudo-second-order kinetic model provided better correlation, with high coefficient of determination value (R^2 ~ 0.9998), than that of pseudo- first-order kinetic model (R^2 ~ 0.9870). Moreover, the calculated qe value derived from pseudo-second-order (table 2) is consistent well with the experimental value, which indicates that the MB adsorption process kinetic on EDTA crosslinked HEC gel was well described by pseudo-second-order kinetic model.

Table 2. Kinetic parameters of pseudo-first-order and pseudo-second-order kinetic models for MB adsorption onto HEC-EDTA gel

	k	qe ($mg.g^{-1}$)	R^2
pseudo- first order	0.132	49.15	0.9870
pseudo-second order	$6.8\ 10^{-3}$	957.9	0.9998

Meanwhile, the study of intraparticle scattering was performed based on Weber-Morries intraparticle diffusion model *(Mabel, Sundararaman et al. 2019)* described by *eq. 10,* where k_{int} is the rate constant of intraparticle diffusion model ($mg.g^{-1}.min^{-1/2}$), and C is a constant involved in the thickness of the boundary layer of the intraparticle diffusion model ($mg.g^{-1}$). Figure 4b shows linear fitted data of intraparticle diffusion kinetic model, where the kinetic parameters (k_{int} and C) were derived from the slope of the linear part of the intraparticle model plots and intersection point at the origin, respectively.

According to the Weber-Morris intraparticle kinetic model, the adsorption process is strictly controlled by intraparticle diffusion if q_t variation against $t^{1/2}$ is a straight line. Therefore, the apparition of three regions of linearity, shown on Fig. 4b, is a strong indication that the intraparticle diffusion is not the only rate-limiting step in the adsorption process. Whereas, the first step *($t^{1/2}$ between 0 and 1 $min^{1/2}$)* showed an interparticle diffusion behavior, characterized by a steep slope *($k_{int(1)}$ = 832 $mg.g^{-1}.min^{-1/2}$),* and correlated to the diffusion of MB from the bulk solution to the boundary layer surrounding on the external adsorption surface of the adsorbent. During first contact, the low recovery rate and the highdensity of active accessible sites, on the external surface of HEC-EDTA (that can be occupied by adsorbate), makes this step the fastest process *(Han, Wang et al. 2011),* and therefore a rate controlling step.

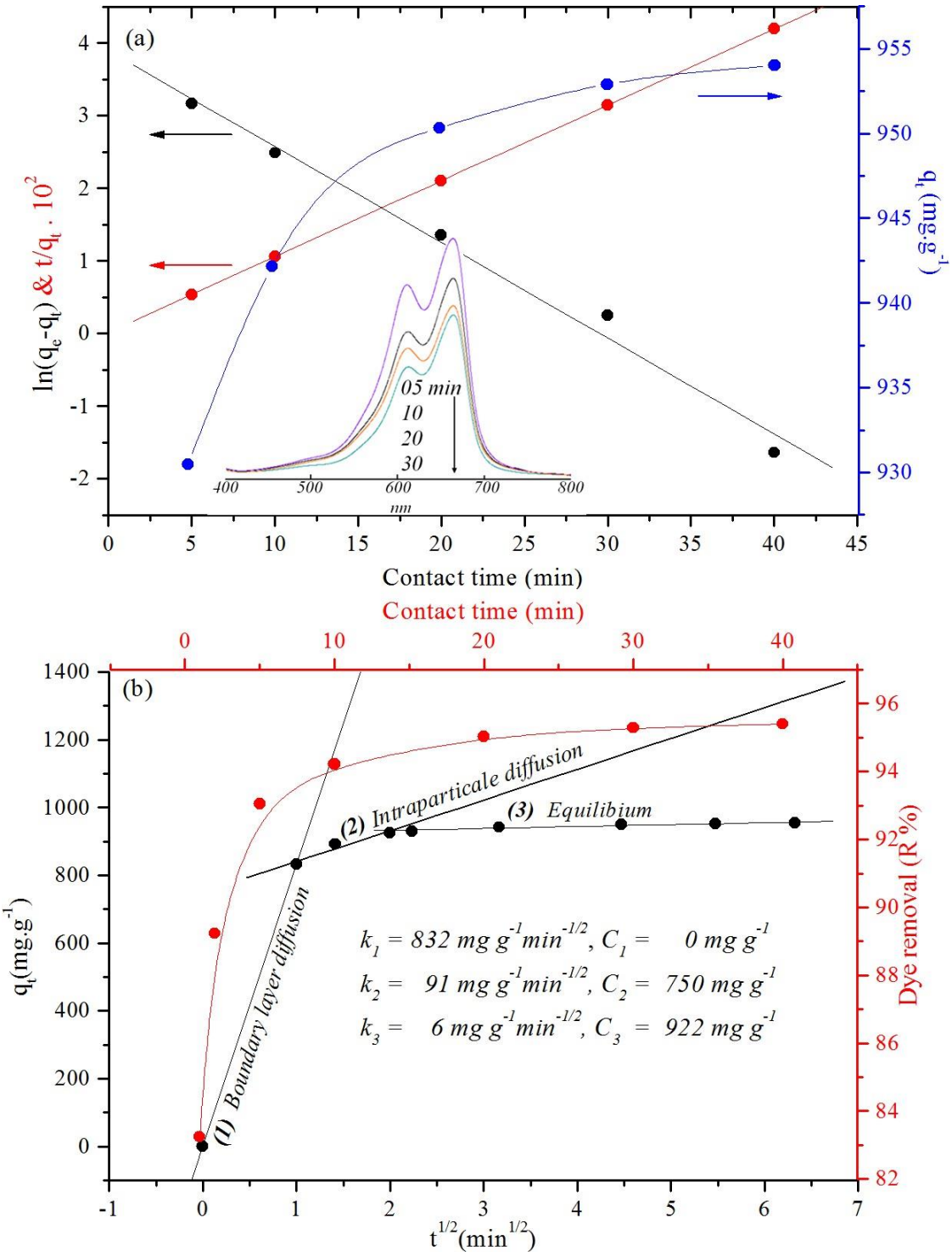

Fig. 4: (a) Contact time effect and kinetic models, (b) intraparticle diffusion model and dye Removal.

The second linear part *($t^{1/2}$ between 1 and 2.5 $min^{1/2}$)* designated by a slight slope *($k_{int(2)}$ = 91 $mg.g^{-1}.min^{-1/2}$)* compared to the previous step, shows the gradual decrease in the adsorption rate, where the change in adsorption process turns from interparticle diffusion to intraparticle one. Indeed, when the gel external surface adsorption sites (HEC-EDTA) are consumed, the adsorbate molecules (MB) penetrate and anchor into the pore sites via an intraparticle diffusion, and this under the osmotic pressure generated by the different concentration gradients of dye molecules in the solution, which drove the filling and diffusion through additional internal surfaces *(Liu, Tian et al. 2019)*. Although, the last linear part showed a very low slope *($k_{int(2)}$ = 6 $mg.g^{-1}.min^{-1/2}$)* indicating the stability of the capacity adsorption, and that the adsorption system has reached equilibrium.

Gel dose, initial concentration and pH effects

The adsorbent dose is an important parameter for enhancing the adsorption capacity for dye removal, and understanding the mechanism profile of the adsorption process. However, the variation of the adsorption capacity (qe) against gel dose *(0.1– 0.6 g.* L^{-1}*,* C_0 *= 600 mg.* L^{-1} *and pH = 8.0)* was illustrated on Figure 5a. However, it can be seen that the adsorption capacity slightly increased with increasing of gel dose from 0.1 to 0.3 g. L^{-1}, where the adsorption capacity moved from 1902 to 1923 $mg.g^{-1}$, while the MB removal ratio (R%) increased from 53.88 % to 73.44 % and to 96.15 % for 0.17, 0.23 and 0.3 g. L^{-1} gel doses, respectively. Then, beyond 0.3 g. L^{-1}, the change in the adsorption capacity of MB is inversely proportional to the gel dose, where the ability to eliminate MB decreased from 1923, 1196 and 1142 $mg.g^{-1}$ to 971 $mg.g^{-1}$ with increasing gelatinous load from 0.3, 0.41, 0.48 to 0.6 g. L^{-1}. In addition, the calculated values of the removal rate (R %), in the adsorbent dose range higher than 0.3 g. L^{-1}, were optimal and greater than 90%.

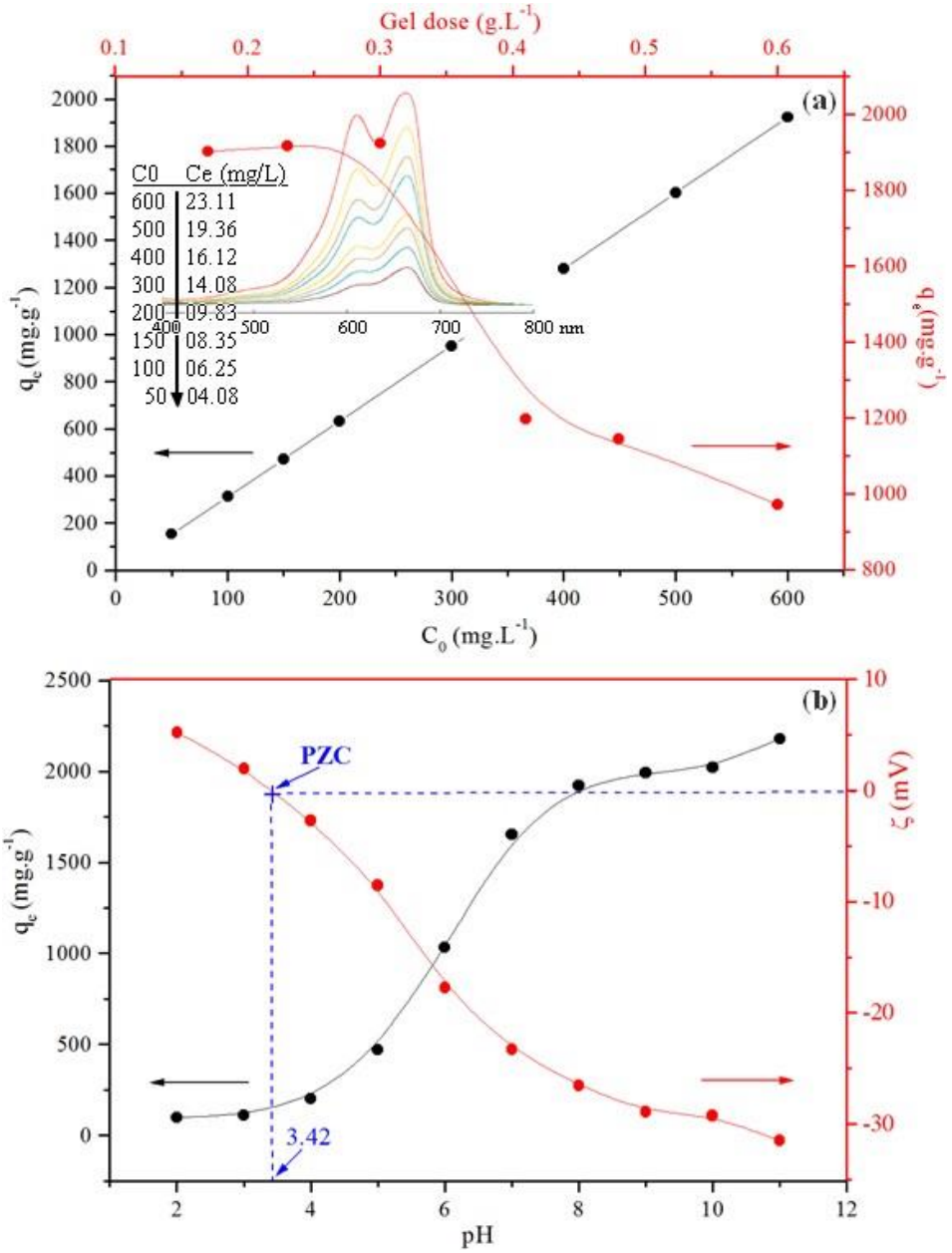

Fig. 5: (a) gel dose and C_0 effects and (b) pH effect on zeta potential of the gel-adsorbent and on adsorption capacity

This behavior can be explained by adsorption resistance, which results from resistance to the mass transfer between external and internal surfaces under osmotic pressure and affects the value of driving forces. Hence, with the high availability of vacant sites, adsorption would easily reach equilibrium. In contrast, more other active sites are not being available because of their aggregation and the lengthening of the diffusion path, consequently, the decrease in the total available surface and the reduction in the adsorption capacity of the material. It is evident that the low rate of recovery of the active sites causes a low adsorption capacity.

In light of this phenomenon, figure 4c shows an overview of the influence of the gel dose on the elimination capacity of MB, so the dose 0.3 g. L^{-1} is selected as an optimal value, indicating that the active sites can be used efficiently, leading to a higher adsorption capacity. The initial dye concentration is another significant factor that determines the effectiveness of the adsorption process. The effect of the initial concentration of the MB solution on the adsorption ability of HEC-EDTA is shown in Fig. 5a, where the experiments were carried out within the initial concentration range of 50 – 600 mg. L^{-1} (25 °C, pH8, gel dose : 0.3 g . L^{-1}). Keeping all the other parameters constant, the results indicate that the adsorption capacity increased linearly over the initial concentration range of 50 – 600 mg. L^{-1}, suggesting that the qe values greatly depended on the initial concentration of MB solution. Indeed, increasing the initial dye concentration induces concentration gradient, generating motrice forces pushing MB towards the adsorbent internal area. On the other hand, more than the difference is significant in MB concentration between the solution bulk and the adsorbent area, the migration rate is greater, where increasing the concentration gradient promotes a high probability of collision between MB molecules and active sites on the adsorbent surface.

Furthermore, in front of the continuous increase of the adsorption capacity against initial concentration of the organic dye, the formation of the multilayers is strongly suggested. This suggestion can be confirmed by the irrationality of models describing the single-layer adsorption, in particular the Langmuir model (Fig. 6a).

The pH of the dye solution is an extensive factor affecting the efficiency of absorption process, where drastically affects both the electrical behavior and the charge density of the adsorbent and the adsorbate, thus governing the adsorbent–adsorbate interaction mechanism. To investigate the pH solution effect on the adsorption efficiency, 0.3 g L^{-1} gel dose 600 mg. L^{-1} MB initial concentration solution at room temperature (25 °C), where the pH solution (2 – 11) was adjusted using HCl and NaOH solution. The results in (Fig. 5b) implied that the adsorption capacity is greatly depending on pH value variation, where at low pH values (2 – 4), low qe values were obtained and attributed to the surface protonation of the adsorbent that indicating a high effect of protonic competition. Above pH = 4, the adsorption capacity increased progressively with an inflection point at ranges of pH6, where the pKa value of the majority of carboxylic acids, indicating the saponification of the carboxylic acid functions, and therefore the activation of active sites in the form of carboxylate functions. At this point, the maximum q_e value was reached and it did not show a significant value change of q_e (2000 – 2150 $mg.g^{-1}$).

To confirm the suggestions previously proposed, the zeta potential of swollen gel at different solution pH was investigated. The results, shown in Figure 5b, indicate that HEC-EDTA hydrogel was characterized by PZC (IEP) corresponding to an isoelectric point of zeta potential at pH = 3.42, where the surface of the adsorbent was neutral and no characteristic adsorption occurred. Considering the typical crosslinking agent and its specificity, EDTA is a hyxaprotonic system representing a distinct proton distribution as a function of pH. The first two acidities of EDTA are anchored to the polymeric chain, which explains its positive zeta potential behavior, which is due to the protonation of the amine forms into ammonium. Therefore, the increase in pH initiated the release of the other two acidities that neutralizes the ammonium charge to the PZC. Beyond that, the adsorption capacity continues to increase, indicating the activation of the active carboxylic sites, reaching 1653 $mg.g^{-1}$ and 1923 $mg.g^{-1}$ at pH values of 7 to 8. At this stage of pH values, the contribution of first structural amine (pKa5 = 6.13) of EDTA to the adsorption mechanism is suggested. This zone is characterized by a strong decrease in zeta potential to a value close to -30 mV, which indicates the predominance of electrostatic interactions in the adsorption mechanism, as well as the carriers of the free doublets, in particular the amine and alcohol functions via sharing of their electronic density. Subsequently, the second structural amine (pKa6 = 10.37) shows practically no activity (weak increase of qe which reaches 2180 $mg.g^{-1}$ at pH = 11), this is due probably to the high alkalinity of the solution where the competitiveness between hydroxide ions and active sites for MB is widely considered.

Adsorption isotherms

The modeling of adsorption isotherms was widely explored to elucidate the adsorbate- adsorbent interactions, as well as for the interpretation of the concentration effect on the dyes adsorption efficiency on solid supports in solution. However, Langmuir, Freundlich, Temkin and Elovich are commonly used isotherm models describing the adsorption phenomenon to understand adsorbate-adsorbent interactions. In the Langmuir isothermal model, the adsorbed molecule is located on a well-defined and specific site of the adsorbent material (localized adsorption), and each site is only capable of binding to one adsorbate-molecule. The adsorption energy distribution of all adsorption sites is identical and independent of theadjacent adsorbed molecules (homogeneous surface and no adsorbate-adsorbate interaction) *(Langmuir 1918)*. Equation 11 gives the linear form of the Langmuir isotherm model.

$$\frac{C_e}{q_e} = \frac{1}{k_l q_m} + \frac{C_e}{q_m} \qquad (Eq. 11)$$

C_e is the MB aqueous solution concentration at equilibrium ($mg.g^{-1}$), qe is the adsorption capacity at equilibrium ($mg.g^{-1}$). k_l is the Langmuir equilibrium constant that indicates the interaction level between the adsorbed molecules and the adsorbent surface, and q_m is the maximum adsorption efficiency ($mg.g^{-1}$). The separation factor is a very useful and characteristic factor of the Langmuir model ($R_l = 1/(1 + K_l C_0)$, the value of $R_l > 1$ indicates that the adsorption is unfavorable, if $0 < R_l < 1$ the adsorption is favorable while the zero value of R_l suggests that the adsorption is irreversible.

The relationship of the classical isothermal Freundlich model is interpreted and proposed first by Saussure, and later popularized by Freundlich *(Freundlich 1907)*. However, the linear form of power function (*Eq. 12*) describing the Freundlich isotherm model is commonly considered an empirical proposition, which gives an excellent description of the experimental isotherms obtained for solution phase adsorption *(Weber Jr, Voice et al. 1983)*. In order to establish a theoretical basis linking the adsorption capacity and the physicochemical or/and molecular properties of adsorbent–adsorbate system, the Freundlich model has excited several lines of research. However, finding a theoretical description and introducing new concepts made the objective, especially order of fractal reaction *(Skopp 2009)*, multilayer adsorption *(Halsey 1948)* and heterogeneity of the binding energy *(Deliyanni, Peleka et al. 2007)* and the surface potential *(Sips 1948)*.

$$lnq_e = lnK_f + \frac{1}{n} lnC_e \quad (eq. 12)$$

Recently, *Na* has shown, based on the Gibbsian interpretation of thermodynamics describing the Freundlich isotherm, that the solution phase adsorption is mainly controlled by the capillary effect of surface tension, and therefore the adsorption capacity can be quantitatively related to the molecular properties of adsorbate. In addition, analyzing the experimental values of 1/n (adsorption intensity, indicates the adsorbate affinity towards the adsorbent) and K_f (Freundlich equilibrium constant) reported in the literature *(Abe, Hayashi et al. 1982, Xia and Ball 1999)*, *Na* demonstrated the linear correlation between the inverse of the Freundlich power, n, and the molecular size of the adsorbate. Hence, the linear correlation between the Freundlich power and the logarithm of the equilibrium constant was discovered, revealing the existence of an isocapacity concentration (ICC) for the adsorption *(Na 2020).*

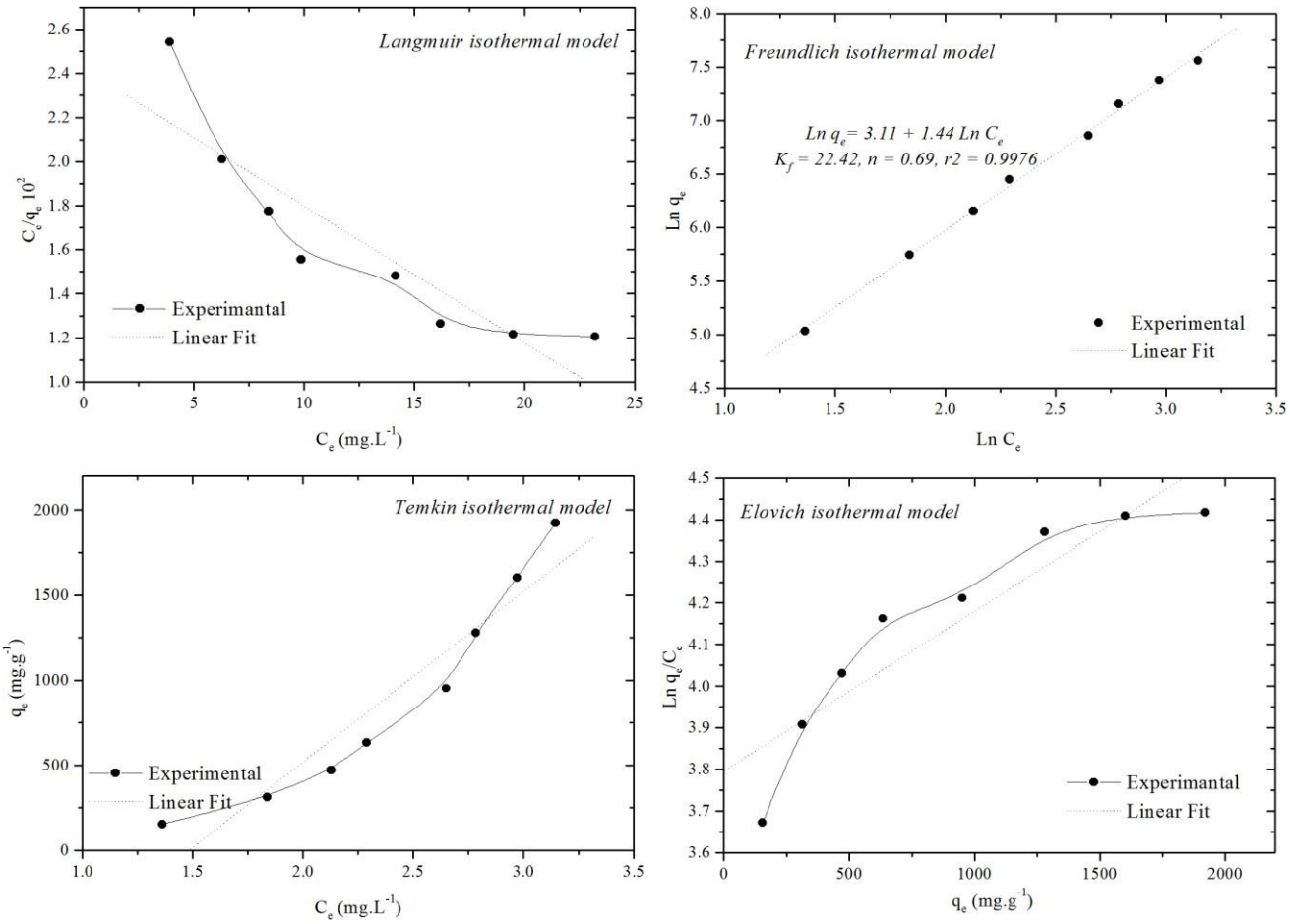

Fig. 6: The experimental results of adsorption of MB on HEC-EDTA illustrated according to Langmuir, Freundlich, Temkin and Elovich theoretical models

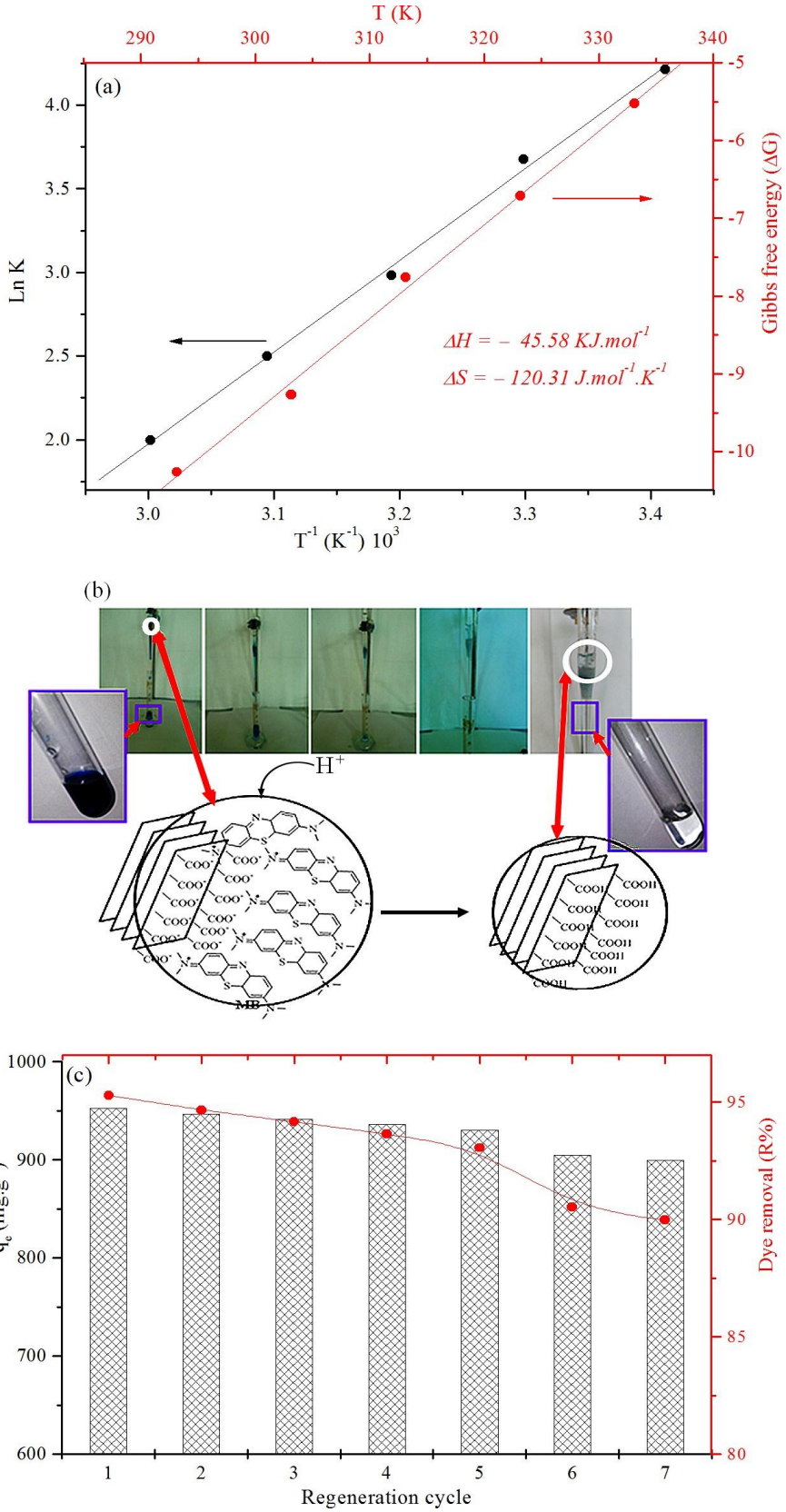

Fig. 7: (a) variation of lnK and ΔG against 1/T and T, (b) Illustration of the regenerability steeps of HEC-EDTA and (c) variation of adsorption and dye removal capacities against regenerability cycle number

Temkin assumes that the heat of adsorption of all molecules in the cover layer decreases linearly with the degree of coverage *(Togue Kamga 2019)*, this variation may be linked to side interactions between adsorbed molecules (adsorbent-adsorbate interactions *(Han,Chakraborty et al. 2022)*. However, the Temkin adsorption isotherm is characterized by a uniform distribution of surface binding energies *(Kavitha and Namasivayam 2007)*. The Temkin isotherm is expressed by equation 13, where, q_e is the equilibrium adsorption efficiency ($mg.g^{-1}$), Ce is the equilibrium adsorbate concentration ($mg.\ L^{-1}$), R is the universal gas constant ($J.mol^{-1}.K^{-1}$), T is the temperature (K), b is the adsorption energy dependence constant and Kt is the equilibrium constant ($L.mg^{-1}$).

$$q_e = \frac{RT}{b} lnK_t + \frac{RT}{b} lnC_e \quad (eq.13)$$

Elovich model differs from that of Langmuir regarding the evolution of adsorption sites, where the density of available sites varies during adsorption, which implies adsorption in several layers *(Hadj Salah 2012)*. The Elovich isotherm is expressed by equation 14 (Eq.14), where q_m ($mg.g^{-1}$) is the maximum adsorption capacity and K_e is the Elovich constant ($m.g^{-1}$).

$$ln\frac{q_e}{C_e} = \frac{q_e}{q_m} + \ln(k_e q_m) \quad (eq.14)$$

Figure 6 illustrates the experimental isothermal results of MB adsorption on HEC-EDTA, fitted according to the theoretical models of Langmuir, Freundlich, Temkin and Elovich. However, a strong correlation was observed for the Freundlich isotherm model, indicating its validity with a high coefficient of determination value (r^2 = 0.9976), which indicates the reliability of the data and a good degree of reproducibility. This great correlation is a strong indication of the heterogeneity of the active surface of the material, and the MB adsorption was carried out in a multi-layer process. This result is in good agreement with the proposed structure where the presence of the different adsorbent sites with heterogenic reactivity in nature. Furthermore, in the crosslinking reaction conditions of HEC by EDTA, especially the value of the average functionality of the crosslinking system ($f = 1.75$), it is highly probable to suggest the formation of a two-dimensional network with different suggested active sites. In particular, the carboxylic functions (-COO-), the amines (-N<) and alcohols (-OH) functions can interact by their free electronic-doublets as negative charges liable to create electrostatic bonds with the MB *(Wang, Zhao et al. 2018, Ning, Zhang et al. 2021).*

The Freundlich constants *(K_f = 22.42 mg.g^{-1})* which is a measure of the degree of adsorption and the exponent of non-linearity (*1/n =1.44)* can be determined from the slope and intercept of the $ln\, qe = f(ln\, Ce)$ plot (linear red curve on Fig. 6). However, the high value of K_f suggests a high degree of heterogeneity *(Somera, Cuazon et al. 2019),* where to interpret the value of 1/n found in this work, it is important to highlight some efforts discussing the relationship between this constant and the mechanism of the adsorption process. Therefore, the value 1/n derived from the Freundlich equation serves to describe the linearity of adsorption, or alternatively the degree of curvature of the isotherms described in the concentration range tested. In a nonlinear mode, the plot is linear for up to 50% max saturation and then becomes nonlinear. Although the Freundlich equation provides essential information regarding the adsorption of particles, but it has limited by the empirical aspect and its validity only up to certain concentrations, above which it becomes nonlinear *(K.Singh 2016)*. However, the Freundlich model linearity has often been attributed to the unit value of the adsorption intensity *(n=1)*. The non-linearity was associated with the hydrophobic behavior and the hydrophobicity degree of the adsorbate molecules, where the adsorption process was controlled by the solubility level *(Carmona, Dal Sasso et al. 2021, Filep, Szabó et al. 2021, Jayalakshmy and Sreethu 2021)*. A unit value of 1/n was assigned to the homogeneous distribution of adsorbent sites, involving a type C isothermal distribution. While, the values ranging from 0.7 to 1.0 showed a decrease in adsorption capacity with increasing the concentration of the adsorbate molecules, which corresponds to the L-type isotherm profile, where much curved isotherms were encountered for 1/n values less than 0.7.

Unusually, values greater than 1 (1/n>1) have been the subject of scientific debate with many gray areas about their meaning, several interpretations of which have been surmounted to the surface. Some authors have linked the small value of n to the competitive effect, at low concentrations, between the different constituents of the adsorbate system or to solvent competition. In the light of this, Wu et al. have shown that systems anionic with the law competitive solute concentrations offer similar n values to that of the single solute (n = 0.33 < 1); this finding suggests that the competitive effect is insignificant when are added in low concentrations *(Wu, Lo et al. 2000, Wu, Kuo et al. 2002)*. A comparison study, performed by *Wu et al.*, of the n values in a single solute system with that in a binary solute system, showed that a more significant competitive effect results in a higher n value but a lower K value *(Wu, Kuo et al. 2002)*. In addition, the same results were observed in the case of Freundlich competitive adsorption, heavy metal adsorption *(Park, Ok et al. 2016, Zhang, Wei et al. 2016,Wang, Liu et al. 2018)* or organic matter adsorption on solid supports *(Yu, Wang et al. 2016, Conde-Cid, Ferreira-Coelho et al. 2019, Wang, Wang et al. 2019, Conde-Cid, Fernández-Sanjurjo et al. 2020)*. Moreover, *Dada et al.* considered the 1/n Freundlich

value to indicate the surface heterogeneity degree, where small values of 1/n indicate that a significant level of heterogeneity is expected *(Dada, Olalekan et al. 2012)*. Further on, *Senthil Kumar et al.* linked the value n<1 to the chemical nature of the adsorption process, while n>1 means the physical process nature of MB dye adsorption onto *sulfuric acid treated Orange Peel (Senthil Kumar, Fernando et al. 2014)*. However, according to *Mohan et al.*, 1/n above one indicates a cooperative adsorption process *(Mohan and Karthikeyan 1997, Dada, Olalekan et al. 2012)*, and is the adsorption validity index if n is between one and ten *(Goldberg 2005)*. At 1/n < 0.1, the adsorption isotherm is irreversible *(Worch 2012, Saadi, Saadi et al. 2015)*, etc. Faced with this ambiguity and the absence of an interpretation based on the acceptable theoretical usefulness of this famous model, almost all of the authors agree that the value of 1/n can classify adsorption isotherms as concave ($1/n > 1$) and convex ($1/n < 1$) functions. The first one showed the direct proportionality of sorption energy to the surface concentration, where the convex demonstrated that the adsorption energy is inversely proportional to the surface concentration *(Can, Ömür et al. 2016)*. In this work is greater, the obtained value for 1/n (1.44) is greater than unity, thus indicating a heterogonous sorption energy distribution.

In addition, S-type adsorption, according to the classification of *Giles et al.* for solution phase adsorption isotherms *(Giles, Smith et al. 1974)*, is the mostly considered to adsorbing adsorbate containing a polar functional group on adsorbent hydrogels. This was observed even for high values of 1/n, which can reach about ten (between 2 and 12) *(Gu and Zhu 1990, Yurdakoç, Seki et al. 2005, Khandelwal, Narayanan et al. 2020)*. This correspondence can be attributed, at low concentrations, to the difference between the force of diffusion (swelling) versus the force of concentration gradient and mass transfer of solute *(Kaşgöz and Durmus 2008, Narayanan, Nethran et al. 2014, Bai, Zhang et al. 2016, Du and Piao 2018, Saraydın, Işıkver et al. 2018)*.

Thermodynamic study and regenerability

The effect of temperature on the adsorption capacity was studied within the temperature range between 20 and 60 ˚C (C0 = 300 mg. L^{-1}, contact time = 30 min, pH8 and 0.3 g. L^{-1}). However, the linear curves representing the thermal profiles of the adsorption equilibrium constant ($lnK = f(1/T)$) and of the Gibbsian energy variation ($\Delta G = f(T)$) are shown in Figure 7a. As can be seen, the increasing temperature was inversely influenced the evolution of *Ln*K, which indicates the increase in the rate constant of the reverse reaction of adsorption, where the adsorption equilibrium moves in the opposite direction. This profile is accompanied by a similar decrease in the adsorption capacity, indicating the physisorption nature of the adsorption process. The stability of the physical adsorbent-adsorbate bonds is low compared to the thermal energy supplied to the

system, and consequently, the breakdown and shift of equilibrium towards favoring desorption. Similarly, the increase in the Gibbs energy (ΔG) value of the adsorption reaction, increasing temperature (Figure 7a), is a strong indication of the physical aspect of the adsorption process. This behavior of free energy confirms the previous result and justifies the changes in the equilibrium constant with temperature. The Gibbs energy change of the adsorption reaction was estimated from Equation 15:

$$\Delta G = -RT\ lnK \qquad (Eq. 15)$$

Where ΔG is the variation of free energy *(KJ. mol^{-1})*, R is the universal gas constant. T is the temperature (K) and *K* is the equilibrium constant. The values of the enthalpy (ΔH) and the entropy (ΔS) can be calculated from the *Van'tHoff Equation* (Eq. 16):

$$lnK = -\frac{\Delta H}{RT} + \frac{\Delta S}{R} \qquad (Eq.\ 16)$$

The thermodynamic parameters of the adsorption, *ΔH* and *ΔS*, can be determined byplotting *LnK=f(1/T)*. The negative values of ΔG confirm the spontaneous behavior of the adsorption process, while the negative enthalpy value of ΔH *(-45.58 KJ.mol^{-1})* shows the exothermic nature of the reaction. In addition, the negative entropy value of ΔS *(- 120.31J.mol^{-1}.k^{-1})* indicates an increase in the molecular order and a significant decrease in the degree of freedom of the solute molecules *(MB)*, when fleeting from the solution to the adsorbent surface connection. The apparent activation energy value (*Ea/R*) was estimated from the experimental data, using the modified Arrhenius equation related to the surface coverage (θ) and the sticking probability, that quantifies the potential of an adsorbate to remain on the adsorbent indefinitely *(Horsfall Jnr and Spiff 2005, Aljeboree, Alkaim et al.2015, Thabet and Ismaiel 2016, Labidi, Salaberria et al. 2019)*. However, the surface coverage was calculated according to the following relation: $\theta = 1- C_e/C_0$, where C_0 and C_e

are initial and equilibrium MB concentrations, respectively. Yet, plotting *ln (1 – θ)* against *1/T* gives a linear plot with a slope of *Ea/R*, which *Ea/R* value was found to be *– 4.7 KJ.g.mol*$^{-1}$. The negative value of *Ea* confirms that the MB adsorption process is exothermic and indicates that lower temperatures were favorable for the MB removal by adsorption using HEC-EDTA adsorbent. Therefore, these results complement the previous ones and confirm that the process of the adsorption of MB is physisorption. In addition, the low values of *Ea* suggest that adsorption is a diffusion-controlled process.

Even with their adsorption efficiency, adsorbents must be inexpensive, regenerated, andpresent a green approach, which encourages their use at the industrial level. Therefore, it is desirable to have economically viable methods for removing cationic dyes, particularly by adsorbents based on environmentally and friendly raw materials. In this context, HEC-EDTA hydrogel has an exceptionally high adsorption capacity for MB. During the adsorbent regeneration step, the procedure of recovering the organic dyes was easily accomplished by eluting the gelatinous mass with adequate 0.1 M aqueous acid solution *(Hu, Liang et al. 2018, Wang, Zhang et al. 2020, Ning, Zhang et al. 2021)*. In this paper, the study of the regenerability and reusability of elaborated HEC based hydrogel, was carried out for 0.5 g of HEC-EDTA-BM (qe ~ 950 mg.g^{-1}) in a 10 mL column, eluted with 0.1 M aqueous HCl solution (Fig. 7b). Figure 7b shows that the upward flow of acid causes discoloration of the adsorbent, where the solution collected at the outlet of the column has become colorless after adding a volume of acid that does not exceed 10 mL. Regeneration results from the release of MB under the action of the acid, which causes the protonation of the carboxylate and amino functions on the surface of the HEC-EDTA adsorbent, and consequently, eliminates the646 electrostatic interactions between MB and HEC -EDTA.

Reusability is one of the crucial properties of the adsorbent for practical application, especially in wastewater treatment dyes removal. The adsorption–desorption flow chart and adsorption–desorption cycles are exhibited in Figure 7c. As shown in Fig. 7c, after five cycles, the adsorption capacity is still maintained at around of the original adsorption capacity. Hence, there was a slight decrease after five consecutive adsorption – desorption cycles (for 6th and 7th cycle), but the dye removal still exceeded 90% to the initial adsorption.High adsorption efficiency and long life cycle of HEC-HEC hydrogel provides promising material as ecofriendly regenerable adsorbent with high-performance and excellent practical value for industrial applications.

Theoretical and Computational Study

Molecular dynamics simulations for the structure materials were conducted using the*Adsorption Locator* module imbedded in *Materials Studio2017* software *(Amrhar, Berisha et al. 2021).* Force field parameterizations were calculated and optimized using COMPASS II *(Biabangard, Nazari et al. 2021).* In this regard, the periodic HEC-EDTA system consists of six monomers HEC oligomers grafted by EDTA, and that according to the experimental discussed results above (degree of substitution *(DS)* and degree of crosslinking *(Dc %)*, where two conjugated bases of carboxylic groups corresponding to each EDTA unit, and *ii)* Cationic MB ions optimized using DFT methods *(Pelalak, Soltani et al. 2021)*. However, the initial charges implemented were *Hirshfeld* charges. The charge partitioning by *Hirshfeld* method shows that S atom has a positive charge of 0.1504e, and N has a negative charge of 0.1471 e *(Li, Zhang et al. 2018).*

Adsorption simulation was carried out in two stages, adsorption of 12 MB+ on the surface of HEC–EDTA layer of six monomers, followed by MD simulations to achieve the optimal results. MD simulations have been conducted as an NPT ensemble giving the experimental conditions *(Guo, Zhang et al. 2020)*. Temperature and pressure were controlled using the *Nose-Hoover* and *Berendsen* method respectively, with all simulations performed at 298.15 K and 1 bar. The motion equations were integrated using the velocity *Verlet* integrator method with a time phase of 1 fs. *Lennard-Jones* encounters were handled with possible 15 Å cut-offs and Periodic boundary conditions have been applied in all directions, and 10 ps long MD Simulations have been used for the studied systems.

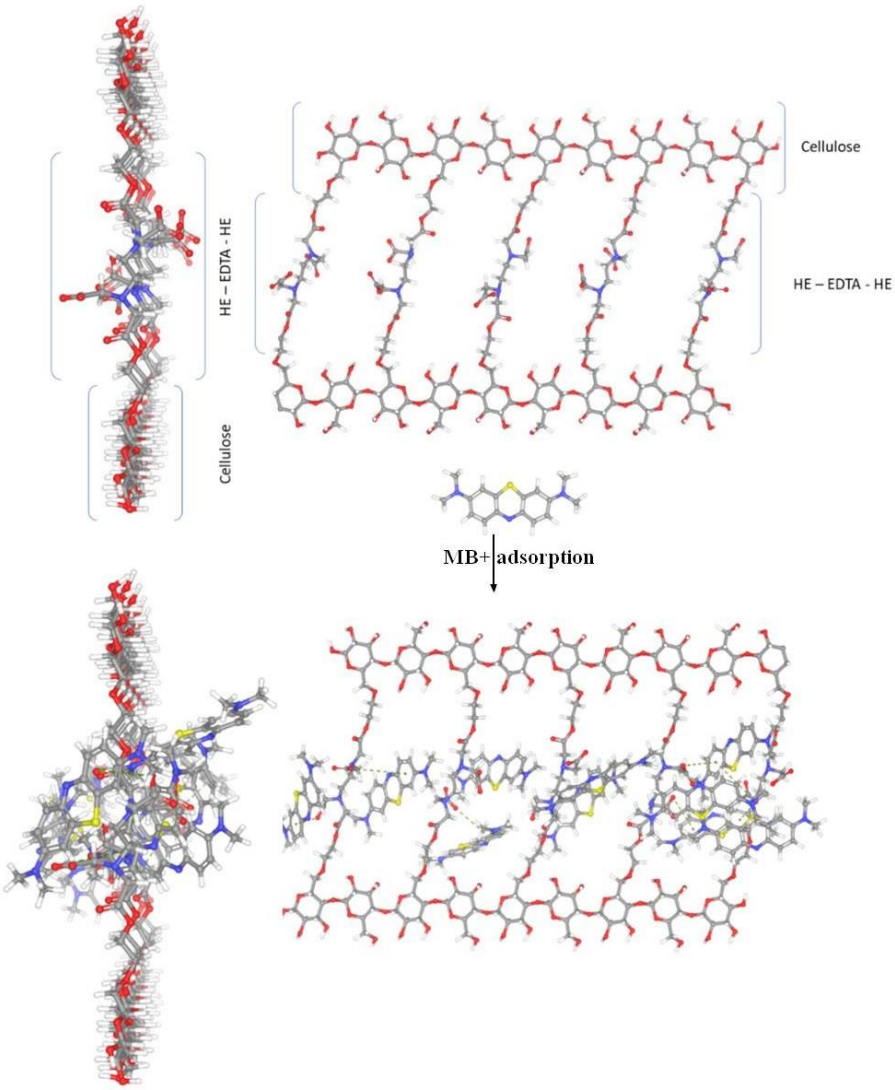

Fig. 8: MD Adsorption simulations of MB+ on HEC EDTA

Intermolecular Non-covalent interaction of MB+ and HEC-EDTA

The molecular structures of MB+ and HEC-EDTA were examined in terms of intermolecular Non-covalent interactions including Pi-Pi interactions, anion-Pi interactions and electrostatic interactions, and sub-structural molecular clusters. However, MD simulation results showed that the adsorption process was better described by non-covalent interactions between methylene blue and carboxylate EDTA entities, especially the electrostatic collisions which given the possibility to create regioselective clusters around EDTA-carboxylates *(Stîngă, Băran et al. 2021)*. At first, the results of MD simulation reveal the tendency of MB+ to be adsorbed on the HEC-EDTA surface, as expected this is due to electrostatic interaction between cationic MB ions and anionic EDTA-carboxylate groups (Fig. 8). The electrostatic interactions (between MB+ and O-) and Pi-cations (between aromatic rings and MB+) led to

the formation of the major molecular clusters. On the other hand, the Pi-Pi interactions (between phenyl groups themselves and between Phenyl groups and carbonyl oxygen) and the Pi-cation interactions (between delocalized MB+ and carboxylic conjugate groups) sustain sub structural clusters *(Khalaf, Hamed et al. 2021)*.

Molecular structure and cluster configurations

Molecular dynamics simulations showed the formation of specific configurations of MB inHEC-EDTA cluster cavities. The region selectivity of MB+ adsorption observed in Fig. 8 is due to non-covalent interactions discussed above, where the repulsive forces between grafted $EDTA^{2-}$ give reason to the apparition of new structural orientations and configurations. These steric arrangements in the new chemical environment induced a new redistribution of bond strengths. The formation of cavities (Fig. 9a) allows the MB+ adsorption in several geometric possibilities (clusters), which explains the high adsorption capacity of HEC-EDTA material to cationic dyes. Yet, the orientation of MB+ was finding selective (i.e. phenyl rings toward O- by anion - Pi interaction) (Fig. 9).

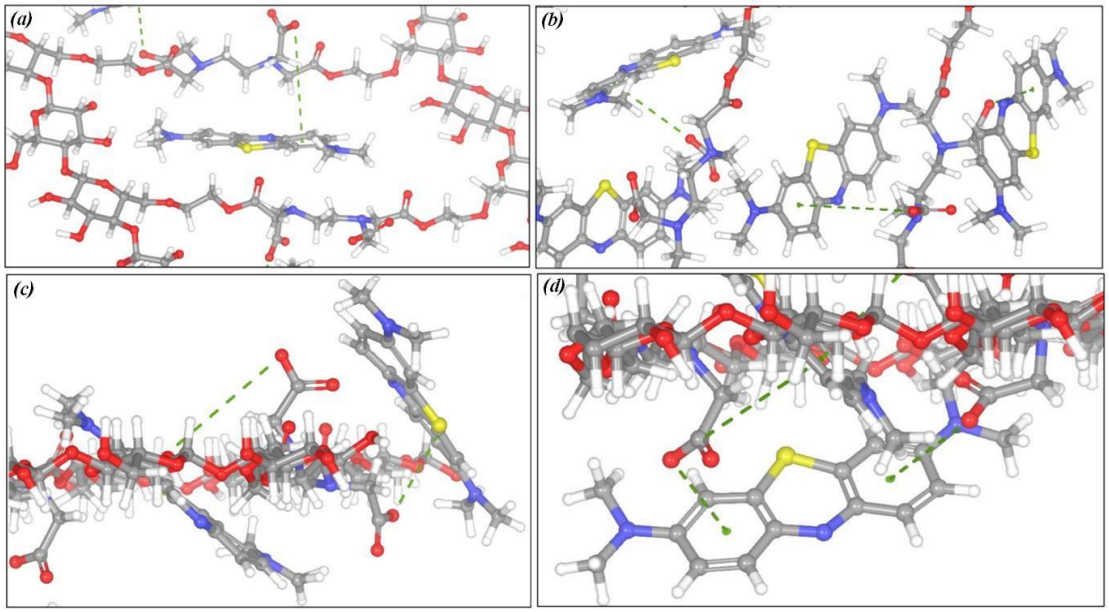

Fig. 9: Submolecular clusters MB-EDTA interactions. (*Dashed lines represent non-covalent interactions*)

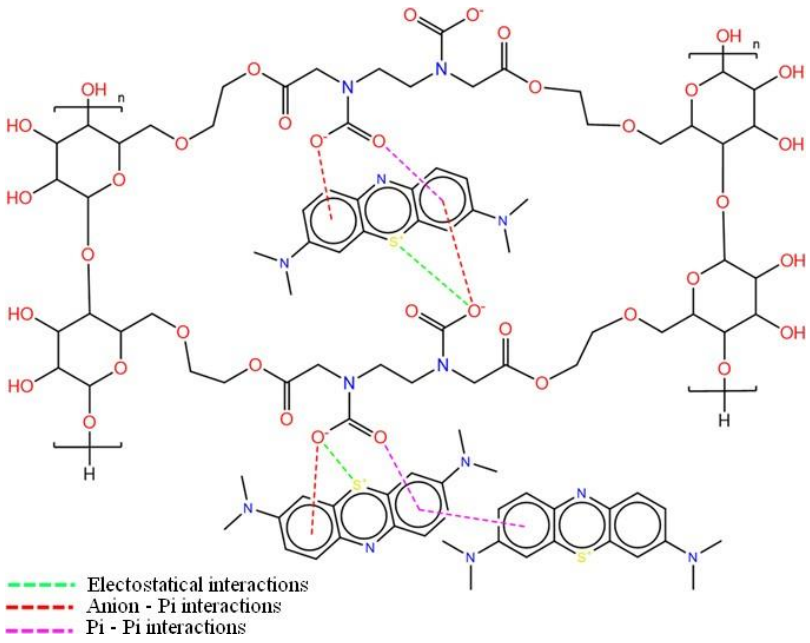

Fig. 10: Proposal MB adsorption mechanism on HEC-EDTA

In addition, the contribution of repulsive forces (i.e. repulsive forces, cation-Pi and Pi-Pi interaction) to the formation of MB+ clusters is strongly suggested (Fig. 10). However, the Pi-Pi interaction of phenyl rings leads to ring stacking, consequently inducing the formation of MB+ aggregates. With regard to the excess repulsive charges, this is compensated by a negative EDTA charge. Thus, the results correlate with experimental evidence and explain them in terms of molecular adsorption, and are in good agreement with those recently published in the literature (Mohammed, Lian et al. 2021).

Conclusion

In this paper, the results of structural analyzes (FTIR and 13C CP/MAS NMR) showed that the synthesis of new pH-sensitive hydrogel (HEC-EDTA) was carried out successfully and applied with good performance as adsorbent of organic micropollutants in aquatic systems. In addition, the mean system functionality around the value 2 (≈ 2/AGU) strongly suggests a 2D-dimensional microstructure of HEC-EDTA, and therefore, sheet morphology is expected with good penetration of pollutant-carrying liquid. The adsorption capacity was studied according to the experimental conditions (pH, contact time, concentration, etc.) in order to optimize the adsorption capacity. In addition, the kinetic study showed pseudo-second-order kinetics while the thermodynamic behavior showed a negative effect of temperature indicating a physical process of adsorption, with an energetic heterogeneity of the surface active sites that

are proven by a strong correlation with the Freundlich model. Molecular dynamics simulations were investigated to confirm the experimental results and the good agreement was shown. The high adsorption efficient of HEC-EDTA to cationic dyes was attributed, basing on the MDs results, to the formation of specific configurations of MB-EDTA clusters, where the non-covalent interactions are predominant. In addition, the repulsive forces between MB entities and between MB and grafted $EDTA^{2-}$ give reason to the apparition of new structural orientations and configurations (electrostatic cavities), thus increase the adsorption efficiency.

Note that this paper is part of a global study on energy storage, where this material hasbeen used as a precursor in the production of cathode compartments of ion batteries, which736 will be published later this year.

Acknowledgements

We thank greatly the anonymous reviewers for their careful review and valuablesuggestions on the manuscript. The authors are thankful to the Head of Oujda's chemistrydepartment, *Prof. Abdelmonaem TALHAOUI*, for providing all the facilities and subsidies necessary to carry out the research work of this article. Our warm thanks are addressed to *Prof. Gharibi EL KHADIR*, Director of the Solid Mineral Solid Chemistry Laboratory –Oujda, for his sincere and persistent contributions and devoted cooperation.

References

Abe I, Hayashi K, Hirashima T and Kitagawa M (1982) Relationship between the Freundlich adsorptionconstants K and 1/N hydrophobic adsorption. Journal of the American Chemical Society 104: 6452-6453.

Al-Kdasi A, Idris A, Saed K and Guan CT (2004) Treatment of textile wastewater by advanced oxidation processes—a review. Global nest: the Int. J 6: 222-230.

Aljeboree AM, Alkaim AF and Al-Dujaili AH (2015) Adsorption isotherm, kinetic modeling and thermodynamics of crystal violet dye on coconut husk-based activated carbon. Desalination and Water Treatment 53: 3656-3667.

Amrhar O, Berisha A, El Gana L, Nassali H and S. Elyoubi M (2021) Removal of methylene blue dye by adsorption onto Natural Muscovite Clay: experimental, theoretical and computational investigation. International Journal of Environmental Analytical Chemistry: 1-26.

Andreozzi R, Caprio V, Insola A and Marotta R (1999) Advanced oxidation processes (AOP) for water

purification and recovery. Catalysis today 53: 51-59.

Bai H, Zhang Q, He T, Zheng G, Zhang G, Zheng L and Ma S (2016) Adsorption dynamics, diffusion and isotherm models of poly (NIPAm/LMSH) nanocomposite hydrogels for the removal of anionic dye Amaranth from an aqueous solution. Applied Clay Science 124: 157-166.

Barclay S and Buckley C (2000) Waste Minimization Guide for the Textile Industry. A step towards cleaner production 1.

Barka N, Qourzal S, Assabbane A, Nounah A and Yhya A-i (2008) Adsorption of Disperse Blue SBL dye by synthesized poorly crystalline hydroxyapatite. Journal of Environmental Sciences 20: 1268-1272.

Beer R, Baumann MA and Kielbassa AM (2006). Endodontia: texto e atlas. Endodontia: texto e atlas: 246-246.

Biabangard F, Nazari H and Arefinia R (2021) Effect of pH on the electrochemical properties of polyaniline nanoparticle suspension in strongly acidic solution: an experimental and theoretical study. Journal of Solid State Electrochemistry 25: 881-893.

Bolotin P, Baranovsky S and Evstigneev M (2006) Spectrophotometric investigation of the hetero-association of Caffeine and thiazine dye in aqueous solution. Spectrochimica Acta Part A: Molecular and Biomolecular Spectroscopy 64: 693-697.

Calcagnile P, Sibillano T, Giannini C, Sannino A and Demitri C (2019) Biodegradable poly (lactic acid)/cellulose-based superabsorbent hydrogel composite material as water and fertilizer reservoir in agricultural applications. Journal of Applied Polymer Science 136: 47546.

Can N, Ömür BC and Altındal A (2016) Modeling of heavy metal ion adsorption isotherms onto metallophthalocyanine film. Sensors and Actuators B: Chemical 237: 953-961.

Cao Y-L, Pan Z-H, Shi Q-X and Yu J-Y (2018) Modification of chitin with high adsorption capacity for methylene blue removal. International journal of biological macromolecules 114: 392-399.

Capretta A, Maharajh RB and Bell RA (1995) Synthesis and characterization of cyclomaltoheptaose-based metal chelants as probes for intestinal permeability. Carbohydrate Research 267: 49-63.

Carmona FJ, Dal Sasso G, Ramírez-Rodríguez GB, Pii Y, Delgado-López JM, Guagliardi A and Masciocchi N (2021) Urea-functionalized amorphous calcium phosphate nanofertilizers: optimizing the synthetic strategy towards environmental sustainability and manufacturing costs. Scientific reports 11: 1-14.

Cenens J and Schoonheydt R (1988) Visible spectroscopy of methylene blue on hectorite, laponite B, and barasym in aqueous suspension. Clays and Clay Minerals 36: 214-224.

Cha C-J, Doerge DR and Cerniglia CE (2001) Biotransformation of Malachite Green by the

FungusCunninghamella elegans. Applied and environmental microbiology 67: 4358-4360.

Chaouf S, El Barkany S, Jilal I, El Ouardi Y, Abou-salama M, Loutou M, El-Houssaine A, El-Ouarghi H, El Idrissi A and Amhamdi H (2019) Anionic reverse microemulsion grafting of acrylamide (AM) on HydroxyEthylCellulose (HEC): synthesis, characterization and application as new ecofriendly low-cost flocculant. Journal of Water Process Engineering 31: 100807.

Chergui S (2010). Dégradation des colorants textiles par procédés d'oxydation avancée basée sur la réaction de Fenton: application à la dépollution des rejets industriels.

Choudhury PR, Majumdar S, Sahoo GC, Saha S and Mondal P (2018) High pressure ultrafiltration CuO/hydroxyethyl cellulose composite ceramic membrane for separation of Cr (VI) and Pb (II) from contaminated water. Chemical Engineering Journal 336: 570-578.

Conde-Cid M, Fernández-Sanjurjo MJ, Ferreira-Coelho G, Fernández-Calviño D, Arias-Estevez M, Núñez-Delgado A and Álvarez-Rodríguez E (2020) Competitive adsorption and desorption of three tetracycline antibiotics on bio-sorbent materials in binary systems. Environmental Research 190: 110003.

Conde-Cid M, Ferreira-Coelho G, Núñez-Delgado A, Fernández-Calviño D, Arias-Estévez M, Álvarez-Rodríguez E and Fernández-Sanjurjo MJ (2019) Competitive adsorption of tetracycline, oxytetracycline and chlortetracycline on soils with different pH value and organic matter content. Environmental research 178: 108669.

Coryell TN (2017) Characterization of Cement Thickening Time Properties and Modeling of Thickening Time. MsT: 34.

Crini G, Badot P, Morin-Crini N and Torri G (2007) Wastewater treatment processes: a recent review of the available ethods. Press universitaires de Franche-Comte (PUFC): 16-62.

Culp S, Beland F, Heflich R, Benson R, Blankenship L, Webb P, Mellick P, Trotter R, Shelton S and Greenlees Ku (2002) Mutagenicity and carcinogenicity in relation to DNA adduct formation in rats fed leucomalachite

green. Mutation Research/Fundamental and Molecular Mechanisms of Mutagenesis 506: 55-63.

Dada A, Olalekan A, Olatunya A and Dada O (2012) Langmuir, Freundlich, Temkin and Dubinin–Radushkevich isotherms studies of equilibrium sorption of Zn2+ unto phosphoric acid modified rice husk. IOSR Journal of Applied Chemistry 3: 38-45.

Danel V (1999). Intoxications aiguës en réanimation, Wolters Kluwer France.

De Guzman N and Balela MDL (2019). Atmospherically Stable Silver Nanowire/Hydroxyethyl Cellulose Films and their Application in Flexible Transparent Touch Screen. Key Engineering Materials, Trans Tech Publ.

Du H and Piao M (2018) Facile preparation of microscale hydrogel particles for high efficiency adsorption of bisphenol A from aqueous solution. Environmental Science and Pollution Research 25: 28562-28571.

Dutta K, Mukhopadhyay S, Bhattacharjee S and Chaudhuri B (2001) Chemical oxidation of methylene blue using a Fenton-like reaction. Journal of hazardous materials 84: 57-71.

Elbedwehy AM and Atta AM (2020) Novel Superadsorbent Highly Porous Hydrogel Based on Arabic Gum and Acrylamide Grafts for Fast and Efficient Methylene Blue Removal. Polymers 12: 338.

Filep T, Szabó L, Kondor AC, Jakab G and Szalai Z (2021) Evaluation of the effect of the intrinsic chemical properties of pharmaceutically active compounds (PhACs) on sorption behaviour in soils and goethite. Ecotoxicology and Environmental Safety 215: 112120.

Freundlich H (1907) Über die adsorption in lösungen. Zeitschrift für physikalische Chemie 57: 385-470.

Gbadamosi S, Famuwagun A and Nnamezie A (2018) Effects of Blanching with Chemical Preservatives on Functional and Antioxidant Properties of Fluted Pumpkin (Telferia occidentalis) Leaf. Nigerian Food Journal 36: 45–57.

Giles CH, Smith D and Huitson A (1974) A general treatment and classification of the solute adsorption isotherm. I. Theoretical. Journal of colloid and interface science 47: 755-765.

Gobi K, Mashitah M and Vadivelu V (2011) Adsorptive removal of methylene blue using novel adsorbent from palm oil mill effluent waste activated sludge: equilibrium, thermodynamics and kinetic studies. Chemical engineering journal 171: 1246-1252.

Goldberg S (2005) Equations and models describing adsorption processes in soils. Chemical processes in soils 8: 489-517.

Greene JC and Baughman GL (1996) Effects of 46 Dyes on Population Growth of Freshwater Green Alga Se/eksfrum capricornutum. Text. Chem. Color 28: 23-30.

Gu T and Zhu B-Y (1990) The S-type isotherm equation for adsorption of nonionic surfactants at the silica gel—water interface. Colloids and surfaces 44: 81-87.

Guo F, Zhang J, Pei J, Zhou B, Falchetto AC and Hu Z (2020) Investigating the interaction behavior between asphalt binder and rubber in rubber asphalt by molecular dynamics simulation. Construction and Building Materials 252: 118956.

Hadj Salah N (2012). Etude de la dégradation photocatalytique de polluants organiques en présence de dioxide de titane, en suspension aqueuse et en lit fixe, Grenoble.

Halsey G (1948) Physical adsorption on non-uniform surfaces. The Journal of chemical physics 16: 931-937.

Hämmer M, Gassmann A, Reller A, von Seggern H, Gutfleisch O, Stauber R and Zimmermann J (2019) Recyclable phosphor films: three water-soluble binder systems enabling the recovery of phosphor powders in white leds. Journal of Electronic Materials 48: 2294-2300.

Han B, Chakraborty A and Saha BB (2022) Isosteric Heats and Entropy of Adsorption in Henry's Law Region for Carbon and MOFs Structures for Energy Conversion Applications. International Journal of Heat and Mass Transfer 182: 122000.

Han X, Wang W and Ma X (2011) Adsorption characteristics of methylene blue onto low cost biomass materia lotus leaf. Chemical Engineering Journal 171: 1-8.

Hasan A, Waibhaw G, Saxena V and Pandey LM (2018) Nano-biocomposite scaffolds of chitosan,

carboxymethyl cellulose and silver nanoparticle modified cellulose nanowhiskers for bone tissue engineering applications. International journal of biological macromolecules 111: 923-934.

Hitz H, Huber W and Reed R (1978) Publication Sponsored by ETAD The Adsorption of Dyes on Activated Sludge. Journal of the Society of Dyers and Colourists 94: 71-76.

Horsfall Jnr M and Spiff AI (2005) Effects of temperature on the sorption of Pb2+ and Cd2+ from aqueous solution by Caladium bicolor (Wild Cocoyam) biomass. Electronic Journal of Biotechnology 8: 43-50.

Hu T-L (1996) Removal of reactive dyes from aqueous solution by different bacterial genera. Water science and technology 34: 89-95.

Hu X-S, Liang R and Sun G (2018) Super-adsorbent hydrogel for removal of methylene blue dye from aqueous solution. Journal of Materials Chemistry A 6: 17612-17624.

Huang F, Chen L, Wang H and Yan Z (2010) Analysis of the degradation mechanism of methylene blue by atmospheric pressure dielectric barrier discharge plasma. Chemical Engineering Journal 162: 250-256.

Huang S, Wu L, Li T, Xu D, Lin X and Wu C (2019) Facile preparation of biomass lignin-based hydroxyethyl cellulose super-absorbent hydrogel for dye pollutant removal. International journal of biological macromolecules 137: 939-947.

Jayalakshmy R and Sreethu K (2021) Nanosuspension: A method for solubility enhancement. J. Med. P'ceutical Allied Sci 10.

Jilal I, El-Barkany S, Bahari Z, Sundman O, El-Idrissi A, Abou-Salama M, Loutou M, Ablouh E and Amhamdi H (2019) New benzyloxyethyl cellulose (BEC) crosslinked EDTA: synthesis, characterization and application for supramolecular self-assembling nanoencapsulation of Pb (II). Materials Today: Proceedings 13: 909-919.

Jilal I, El Barkany S, Bahari Z, Sundman O, El Idrissi A, Abou-Salama M, Romane A, Zannagui C and Amhamdi H (2018) New quaternized cellulose based on hydroxyethyl cellulose (HEC) grafted EDTA: synthesis, characterization and application for Pb (II) and Cu (II) removal. Carbohydrate polymers 180: 156-167.

Jilal I, El Barkany S, Bahari Z, Sundman O, El Idrissi A, Salhi A, Abou-Salama M, Loutou M and Amhamdi H (2018) Unconventional synthesis, characterization and theoretical study (HF and DFT computations) of new cellulosic copper complex: benzyloxyethyl cellulose copper (CuBEC). Cellulose 25: 4375-4388.

Jin T, Easton CD, Yin H, de Vries M and Hao X (2018) Triethylenetetramine/hydroxyethyl cellulose-functionalized graphene oxide monoliths for the removal of copper and arsenate ions. Science and Technology of advanced MaTerialS 19: 381-395.

Júnior OK, Gurgel LVA, de Freitas RP and Gil LF (2009) Adsorption of Cu (II), Cd (II), and Pb (II) from aqueous single metal solutions by mercerized cellulose and mercerized sugarcane bagasse chemically modified with EDTA dianhydride (EDTAD). Carbohydrate Polymers 77: 643-650.

K.Singh A (2016) Engineered Nanoparticles Structure, Properties and Mechanisms of Toxicity. Engineered Nanoparticles Structure, Properties and Mechanisms of Toxicity: 343-450. DOI: 10.1016/B978-0-12-801406-6.00008-X.

Kaşgöz H and Durmus A (2008) Dye removal by a novel hydrogel-clay nanocomposite with enhanced swelling properties. Polymers for Advanced Technologies 19: 838-845.

Kavitha D and Namasivayam C (2007) Experimental and kinetic studies on methylene blue adsorption by coir pith carbon. Bioresource Technology 98: 14-21.

Kellner-Rogers JS, Taylor JK, Masud AM, Aich N and Pinto AH (2019) Kinetic and thermodynamic study of methylene blue adsorption onto chitosan: insights about metachromasy occurrence on wastewater remediation. Energy, Ecology and Environment 4: 85-102. DOI: 10.1007/s40974-019-00116-7.

Khalaf B, Hamed O, Jodeh S, Hanbali G, Bol R, Dagdag O and Samhan S (2021) Novel, Environment-Friendly Cellulose-Based Derivatives for Tetraconazole Removal from Aqueous Solution. Polymers 13: 450.

Khandelwal A, Narayanan N, Varghese E and Gupta S (2020) Linear and nonlinear isotherm models and error analysis for the sorption of kresoxim-methyl in agricultural soils of India. Bulletin of environmental

contamination and toxicology: 1-8.

Labidi A, Salaberria AM, Fernandes S, Labidi J and Abderrabba M (2019) Functional chitosan derivative and chitin as decolorization materials for methylene blue and methyl orange from aqueous solution. Materials 12: 361.

Langmuir I (1918) The adsorption of gases on plane surfaces of glass, mica and platinum. Journal of the American Chemical society 40: 1361-1403.

Li H, Lin Y, Luo Y, Yu P and Hou L (2011) Relating organic fouling of reverse osmosis membranes to adsorption during the reclamation of secondary effluents containing methylene blue and rhodamine B. Journal of hazardous materials 192: 490-499.

Li M-C, Mei C, Xu X, Lee S and Wu Q (2016) Cationic surface modification of cellulose nanocrystals: Toward tailoring dispersion and interface in carboxymethyl cellulose films. Polymer 107: 200-210.

Li Y, Zhang X, Chen D, Xiao S and Tang J (2018) Adsorption behavior of COF2 and CF4 gas on the MoS2 monolayer doped with Ni: a first-principles study. Applied Surface Science 443: 274-279.

Liu X, Tian J, Li Y, Sun N, Mi S, Xie Y and Chen Z (2019) Enhanced dyes adsorption from wastewater via Fe3O4 nanoparticles functionalized activated carbon. Journal of hazardous materials 373: 397-407.

Liu X, Wang C, Wang A, Qu J, Wen Y and Wei B (2019) Application of cellulose and cellulose nanofibers in oil exploration. Paper and Biomaterials 4: 69.

Luo P, Liu L, Xu W, Fan L and Nie M (2018) Preparation and characterization of aminated hyaluronic acid/oxidized hydroxyethyl cellulose hydrogel. Carbohydrate polymers 199: 170-177.

Ma Y, Gong X, Liao C, Geng X, Wang C and Chu F (2018) Preparation and characterization of DOPO-ITA modified ethyl cellulose and its application in phenolic foams. Polymers 10: 1049.

Mabel M, Sundararaman T, Parthasarathy N and Rajkumar J (2019) Chitin Beads from Peneaus sp. Shells as a Biosorbent for Methylene Blue Dye Removal. Polish Journal of Environmental Studies 28.

Malik PK (2003) Use of activated carbons prepared from sawdust and rice-husk for adsorption of acid dyes: a case study of Acid Yellow 36. Dyes and pigments 56: 239-249.

Marr HE, Stewart JM and Chiu M (1973) The crystal structure of methylene blue pentahydrate. Acta Crystallographica Section B: Structural Crystallography and Crystal Chemistry 29: 847-853.

Mckay G, Ramprasad G and Mowli P (1987) Desorption and regeneration of dye colours from low-cost materials. Water Research 21: 375-377.

Melo BC, Paulino FA, Cardoso VA, Pereira AG, Fajardo AR and Rodrigues FH (2018) Cellulose nanowhiskers improve the methylene blue adsorption capacity of chitosan-g-poly (acrylic acid) hydrogel. Carbohydrate polymers 181: 358-367.

Mohammed N, Lian H, Islam MS, Strong M, Shi Z, Berry RM, Yu H-Y and Tam KC (2021) Selectiveadsorption and separation of organic dyes using functionalized cellulose nanocrystals. Chemical Engineering Journal 417: 129237.

Mohan SV and Karthikeyan J (1997) Removal of lignin and tannin colour from aqueous solution by adsorption onto activated charcoal. Environmental Pollution 97: 183-187.

Na C (2020) Size-controlled capacity and isocapacity concentration in Freundlich adsorption. ACS omega 5:13130-13135.

Naderi A, Lindström T, Sundström J, Pettersson T, Flodberg G and Erlandsson J (2015) Microfluidized

carboxymethyl cellulose modified pulp: a nanofibrillated cellulose system with some attractive properties. Cellulose 22: 1159-1173.

Naidja L (2010) Elimination du colorant orange II en solution aqueuse, par voie photochimique et par adsorption.

Narayanan RK, Nethran NK, Devaki SJ and Rao TP (2014) Robust polymeric hydrogel using rod-like amidodiol as crosslinker: Studies on adsorption kinetics and mechanism using dyes as adsorbate. Journal of Applied Polymer Science 131.

Ning F, Zhang J, Kang M, Ma C, Li H and Qiu Z (2020) Hydroxyethyl cellulose hydrogel modified with tannic acid as methylene blue adsorbent. Journal of Applied Polymer Science 138: 49880.

Ning F, Zhang J, Kang M, Ma C, Li H and Qiu Z (2021) Hydroxyethyl cellulose hydrogel modified with tannic acid as methylene blue adsorbent. Journal of Applied Polymer Science 138: 49880.

Pagga U and Brown D (1986) The degradation of dyestuffs: Part II Behaviour of dyestuffs in aerobic biodegradation tests. Chemosphere 15: 479-491.

Pan Y, Wang J, Sun C, Liu X and Zhang H (2016) Fabrication of highly hydrophobic organic–inorganic hybrid magnetic polysulfone microcapsules: A lab-scale feasibility study for removal of oil and organic dyes from environmental aqueous samples. Journal of hazardous materials 309: 65-76.

Park J-H, Ok YS, Kim S-H, Cho J-S, Heo J-S, Delaune RD and Seo D-C (2016) Competitive adsorption of heavy metals onto sesame straw biochar in aqueous solutions. Chemosphere 142: 77-83.

Pelalak R, Soltani R, Heidari Z, Malekshah RE, Aallaei M, Marjani A, Rezakazemi M, Kurniawan TA and Shirazian S (2021) Molecular dynamics simulation of novel diamino-functionalized hollow mesosilica spheres for adsorption of dyes from synthetic wastewater. Journal of Molecular Liquids 322: 114812.

Pradeep T (2009) Noble metal nanoparticles for water purification: a critical review. Thin solid films 517: 6441-6478.

Rafatullah M, Sulaiman O, Hashim R and Ahmad A (2010) Adsorption of methylene blue on low-cost adsorbents: a review. Journal of hazardous materials 177: 70-80.

Rager T, Geoffroy A, Hilfiker R and Storey JM (2012) The crystalline state of methylene blue: a zoo of hydrates. Physical Chemistry Chemical Physics 14: 8074-8082.

Rao Z, Ge H, Liu L, Zhu C, Min L, Liu M, Fan L and Li D (2018) Carboxymethyl cellulose modified graphene oxide as pH-sensitive drug delivery system. International journal of biological macromolecules 107: 1184-1192.

Saadi R, Saadi Z, Fazaeli R and Fard NE (2015) Monolayer and multilayer adsorption isotherm models for sorption from aqueous media. Korean Journal of Chemical Engineering 32: 787-799.

Saraydın D, Işıkver Y and Karadağ E (2018) A Study on the correlation between adsorption and swelling for poly (Hydroxamic Acid) hydrogels-triarylmethane dyes systems. Journal of Polymers and the Environment 26: 3924-3936.

Sbai G, Oukili K and Loukili M (2016) Etude de la dégradation des colorants de textile application sur le Bleu de Méthylène [Study of the degradation of the colouring agents of textile application on the Methylene blue]. International Journal of Innovation and Applied Studies 16: 272.

Senna AM, Novack KM and Botaro VR (2014) Synthesis and characterization of hydrogels from cellulose acetate by esterification crosslinking with EDTA dianhydride. Carbohydrate polymers 114: 260-268.

Senna AM, Novak KM, do Carmo JB and Botaro VR (2013) Synthesis and characterization of hydrogels from cellulose acetate by esterification crosslinking with EDTA dianhydride. Blucher Chemistry Proceedings 1:300-300.

Senthil Kumar P, Fernando PSA, Ahmed RT, Srinath R, Priyadharshini M, Vignesh A and Thanjiappan A (2014) Effect of temperature on the adsorption of methylene blue dye onto sulfuric acid–treated orange peel. Chemical Engineering Communications 201: 1526-1547. Silverstein R, Bassler G and Morrill T (1991). Spectrometric identification of organic molecules, John Wiley and Sons, NY, USA. Google Scholar.

Sips R (1948) On the structure of a catalyst surface. The journal of chemical physics 16: 490-495.

Skopp J (2009) Derivation of the Freundlich adsorption isotherm from kinetics. Journal of Chemical Education 86: 1341.

Somera LR, Cuazon R, Cruz JK and Diaz LJ (2019). Kinetics and isotherms studies of the adsorption of Hg (II) onto iron modified montmorillonite/polycaprolactone nanofiber membrane. IOP Conference Series: Materials Science and Engineering, IOP Publishing.

Stîngă G, Băran A, Iovescu A, Brânzoi F and Anghel D-F (2021) Impact of cationic surfactant on fluorescent complex of pyrene labeled poly (acrylic acid) and methylene blue. Journal of Molecular Liquids 322:114545.

Sukumaran VS and Ramalingam A (2011) Third Order Optical Nonlinearities and Spectral Characteristics of Methylene Blue. J. Quantum Information Science 1: 69-72.

Tabaght FE, El idrissi A, Aqil M, Benahemad A, El barkany S, Bellaouchi R and Asehraou A synthesis and characterization of (thio) carbamates based on cellulose and cellulose acetate: biodegradation and solubility studies.

Tenorio-Alfonso A, Sánchez MC and Franco JM (2019) Synthesis and mechanical properties of bio-sourced polyurethane adhesives obtained from castor oil and MDI-modified cellulose acetate: Influence of cellulose acetate modification. International Journal of Adhesion and Adhesives 95: 102404.

Thabet MS and Ismaiel AM (2016) Sol-Gel γ-Al 2 O 3 Nanoparticles Assessment of the Removal of Eosin Yellow Using: Adsorption, Kinetic and Thermodynamic Parameters. Journal of Encapsulation and Adsorption Sciences 6: 70.

Togue Kamga F (2019) Modeling adsorption mechanism of paraquat onto Ayous (Triplochiton scleroxylon) wood sawdust. Applied Water Science 9: 1-7.

Tsuda S, Matsusaka N, Madarame H, Ueno S, Susa N, Ishida K, Kawamura N, Sekihashi K and Sasaki YF (2000) The comet assay in eight mouse organs: results with 24 azo compounds. Mutation Research/Genetic Toxicology and Environmental Mutagenesis 465: 11-26.

Uddin MT, Islam MA, Mahmud S and Rukanuzzaman M (2009) Adsorptive removal of methylene blue by tea waste. Journal of Hazardous Materials 164: 53-60.

Vandevivere PC, Bianchi R and Verstraete W (1998) Treatment and reuse of wastewater from the textile wet-processing industry: Review of emerging technologies. Journal of Chemical Technology & Biotechnology:International Research in Process, Environmental AND Clean Technology 72: 289-302.

Wang G, Zhang J, Lin S, Xiao H, Yang Q, Chen S, Yan B and Gu Y (2020) Environmentally friendly nanocomposites based on cellulose nanocrystals and polydopamine for rapid removal of organic dyes in aqueous solution. Cellulose 27: 2085-2097.

Wang H, Wang B, Li J and Zhu T (2019) Adsorption equilibrium and thermodynamics of acetaldehyde/acetone on activated carbon. Separation and Purification Technology 209: 535-541.

Wang W, Zhao Y, Bai H, Zhang T, Ibarra-Galvan V and Song S (2018) Methylene blue removal from water using the hydrogel beads of poly (vinyl alcohol)-sodium alginate-chitosan-montmorillonite. Carbohydrate polymers 198: 518-528.

Wang X, He J, Ma L, Yan B, Shi L and Ran R (2020) Self-assembling graphene oxide/modified amphipathic hydroxyethyl cellulose hybrid stabilized Pickering emulsion polymerization for functional hydrogel. Colloids and Surfaces A: Physicochemical and Engineering Aspects: 125742.

Wang Y-Y, Liu Y-X, Lu H-H, Yang R-Q and Yang S-M (2018) Competitive adsorption of Pb (II), Cu (II), and Zn (II) ions onto hydroxyapatite-biochar nanocomposite in aqueous solutions. Journal of Solid State Chemistry 261: 53-61.

Weber Jr WJ, Voice TC, Pirbazari M, Hunt GE and Ulanoff DM (1983) Sorption of hydrophobic compounds by sediments, soils and suspended solids—II. Sorbent evaluation studies. Water Research 17: 1443-1452.

Weng C-H and Pan Y-F (2007) Adsorption of a cationic dye (methylene blue) onto spent activated clay. Journal of Hazardous Materials 144: 355-362.

Wilson TM (1907) On the chemistry and staining properties of certain derivatives of the methylene blue group when combined with eosin. The Journal of experimental medicine 9: 645.

Worch E (2012) Adsorption Equilibrium: General Aspects and Single-Solute Adsorption. Adsorption Technology in Water Treatment-Fundamentals, Processes, and Modeling: 42-76.

Wu C-H, Kuo C-Y, Lin C-F and Lo S-L (2002) Modeling competitive adsorption of molybdate, sulfate, selenate, and selenite using a Freundlich-type multi-component isotherm. Chemosphere 47: 283-292.

Wu C-H, Lo S-L and Lin C-F (2000) Competitive adsorption of molybdate, chromate, sulfate, selenate, and selenite on γ-Al2O3. Colloids and Surfaces A: Physicochemical and Engineering Aspects 166: 251-259.

Xia G and Ball WP (1999) Adsorption-partitioning uptake of nine low-polarity organic chemicals on a natural sorbent. Environmental science & technology 33: 262-269.

Yang X, Li Z, Liu H, Ma L, Huang X, Cai Z, Xu X, Shang S and Song Z (2020) Cellulose-based polymeric emulsifier stabilized poly (N-vinylcaprolactam) hydrogel with temperature and pH responsiveness.

International Journal of Biological Macromolecules 143: 190-199. Younes MM, El-sharkawy II, Kabeel A, Uddin K, Pal A, Mitra S, Thu K and Saha BB (2019) Synthesis and characterization of silica gel composite with polymer binders for adsorption cooling applications. International Journal of Refrigeration 98: 161-170.

Yu S, Wang X, Ai Y, Tan X, Hayat T, Hu W and Wang X (2016) Experimental and theoretical studies on competitive adsorption of aromatic compounds on reduced graphene oxides. Journal of Materials Chemistry A 4: 5654-5662.

Yurdakoç M, Seki Y, Karahan S and Yurdakoç K (2005) Kinetic and thermodynamic studies of boron removal by Siral 5, Siral 40, and Siral 80. Journal of Colloid and Interface Science 286: 440-446.

Zafar S, Aqil F and Ahmad I (2007) Metal tolerance and biosorption potential of filamentous fungi isolated from metal contaminated agricultural soil. Bioresource technology 98: 2557-2561.

Zannagui C, Amhamdi H, El Barkany S, Jilal I, Sundman O, Salhi A, Chaouf S, Abou-Salama M, El Idrissi A and Zaghrioui M (2020) Design, Characterization and Investigation of Heavy Metal Ions Removal by New Cellulose-Ether Based adsorbent. Moroccan Journal of Chemistry 8: 8-1 (2020) 2332-2346.

Zare EN, Motahari A and Sillanpää M (2018) Nanoadsorbents based on conducting polymer nanocomposites with main focus on polyaniline and its derivatives for removal of heavy metal ions/dyes: A review. Environmental research 162: 173-195.

Zhang L, Wei J, Zhao X, Li F, Jiang F, Zhang M and Cheng X (2016) Competitive adsorption of strontium and cobalt onto tin antimonate. Chemical Engineering Journal 285: 679-689.

Zhi Z, Ma B, Jian S, Guo Y, Yu H, Tan H and Chen F (2017) Thermal analyses. Journal of Thermal Analysis and Calorimetry 129: 1547-1554.